https://rbgeomorfologia.org.br/
ISSN 2236-5664

Revista Brasileira de Geomorfologia

v. 25, nº 1 (2024)

http://dx.doi.org/10.20502/rbg.v25i1.2427

Temporal trends in sand bars and water bodies on the right side of the world's largest fluvial island - Javaés River

Tendências temporais nas barras arenosas e massas de água na borda direita da maior ilha fluvial do mundo - rio Javaés

Daniel Araújo Ramos dos Santos [1], Édipo Henrique Cremon [2] and Luis Felipe Soares Cherem [3]

[1] Federal University of Goiás (UFG), Institute of Socio-Environmental Studies (IESA), Goiânia, Brazil. daniel.a.sants@hotmail.com
ORCID: https://orcid.org/0000-0001-5934-5239

[2] Federal Institute of Goiás (IFG), Department of Geomatics, Goiânia, Brazil. edipo.cremon@ifg.edu.br
ORCID: https://orcid.org/0000-0003-3174-7273

[3] Federal University of Minas Gerais, Institute of Geosciences, Belo Horizonte, Brazil. lfcherem@ufmg.br
ORCID: https://orcid.org/0000-0002-4119-6690

Received: 14/06/2023; Accepted: 08/12/2023; Published: 30/01/2024

Abstract: Bananal Island is the largest river island in the world, located in the Araguaia River basin in central-western Brazil. Studies on the Araguaia River have shown that changes in the main channel are linked to the increase in sediment input due to agricultural expansion in the Cerrado. However, very little is known about the Javaés River, on the opposite margin of Bananal Island. This study analyzed the temporal trends of sand bars and water masses in the Javaés River from 1985 to 2021. Annual mosaics of Landsat images were generated to identify the classes of water masses and sand bars. The Mann Kendall and Sen's Slope tests were used to identify trends and statistical significance of changes over time. The results indicated an increase of 57% (6.5 km²) in the areas of sand bars and a reduction of 39% (15.2 km²) in water bodies. The tests revealed significant trends with an increase in bars and a decrease in water bodies. It was observed that changes in the distribution and rates of regional precipitation, along with the expansion of anthropogenic occupation, are contributing to an increase in sediment input, in a cascade effect, affecting the balance between erosion and deposition in the Javaés River.

Keywords: River dynamics; River system connectivity; Morphosedimentary balance; Sediment input; Cerrado.

Resumo: A Ilha do Bananal é a maior ilha fluvial do mundo, localizada na bacia do rio Araguaia, Centro-Oeste do Brasil. Estudos no rio Araguaia mostram que mudanças no canal principal estão ligadas ao aumento do aporte sedimentar devido à expansão agrícola no Cerrado. Porém, pouco se sabe sobre o rio Javaés, na margem oposta da Ilha do Bananal. Este estudo analisou as tendências temporais das barras arenosas e massas de água no rio Javaés de 1985 a 2021. Foram gerados mosaicos anuais de imagens Landsat para identificar as classes de massas de água e barras arenosas. Os testes de Mann Kendall e *Sen's Slope* foram utilizados para identificar tendências e significância estatística das mudanças ao longo do tempo. Os resultados indicam aumento de 57% (6,5 km²) nas áreas de barras arenosas e redução de 39% (15,2 km²) nas massas de água. Os testes revelaram tendências significativas com aumento das barras e diminuição das massas de água. Foi observado que mudanças na distribuição e nas taxas de precipitação regional, juntamente com a expansão da ocupação antrópica, estão contribuindo para um aumento no aporte sedimentar, em um efeito cascata, afetando o equilíbrio entre erosão e deposição no rio Javaés.

Palavras-chave: Dinâmica fluvial; Conectividade do sistema fluvial; Equilíbrio morfossedimentar; Aporte sedimentar; Cerrado.

1. Introduction

Rivers are influenced by several external factors, which individually or collectively can cause gradual or pulsating imbalances in their systems, mainly affecting their morphology (BRIERLEY; FRYIRS, 2005; STEVAUX; LATRUBESSE, 2017; BARROS; MAGALHÃES JÚNIOR; COTA, 2020). In tropical regions, reduced rainfall has affected fluvial discharge, increasing levels of deposition in alluvial zones (GOMES et al., 2022), while extreme rainfall events can intensify soil erosion in headwater zones (CHEN; TFWALA; TSAI, 2020; DE HIPT et al., 2018; DIODATO et al., 2020).

Anthropogenic actions can also influence the morphodynamic processes of rivers, especially engineering works, which alter the flow and reduce longitudinal hydrogeomorphological connectivity (GRILL et al., 2019; MACHADO; DOS SANTOS, 2020; ROY, 2022; VERCRUYSSE; GRABOWSKI, 2021). The suppression of riparian vegetation also impacts the stability of river shapes, sinuosity, and width (BEST, 2019; IELPI et al., 2022), and the replacement of native vegetation with agricultural areas increases runoff and erosion rates, reducing evapotranspiration (ANACHE et al., 2019; COE et al., 2011, 2017; MARENGO et al., 2022).

Several techniques have been used to both map and quantify changes in river morphology at different spatial and temporal scales, such as procedures based on biological, historical and planimetric evidence (GURNELL; DOWNWARD; JONES, 1994; LAWLER, 1993). Among these techniques, the interpretation of aerial photographs and historical maps can be highlighted (GILVEAR; WINTERBOTTOM, 1992; HOOKE, 1979, 1980; LATRUBESSE et al., 2009), and planimetric surveys in the field with morphostratigraphic descriptions and monitoring with reference pins (CASTRO; CAMPOS; ZANCOPÉ, 2019; SILVA; SOUZA FILHO; NEVES, 2011).

Throughout the years, two-dimensional river mapping techniques have evolved with the improvement of remote sensing and the development of mapping protocols, such as apps and toolboxes for GIS (Geographic Information Systems) (ISIKDOGAN; BOVIK; PASSALACQUA, 2017; MONEGAGLIA et al., 2018), disseminating work routines that seek to standardize metrics for comparison (NYBERG et al., 2015; SUIZU; LATRUBESSE; BAYER, 2023). The increased accessibility of large historical collections of orbital records, using platforms such as Google Earth and Google Earth Engine, has allowed a significant expansion of the scope of these mappings, and coupled with field approaches, has enabled a multi-scalar overview of channel processes (BOOTHROYD et al., 2021; LANGHORST; PAVELSKY, 2023; VERCRUYSSE; GRABOWSKI, 2021). Understanding the spatial and temporal variation in two-dimensional morphology in rivers has attracted more geomorphological research, as it provides insights into fluvial behavior and indicates river responses to endogenous and exogenous changes (AGNIHOTRI; OHRI; MISHRA, 2020; SCHUMM, 1985; WANG et al., 2016).

The changes in two-dimensional morphology in multichannel river systems, which typically characterize the world's largest rivers, are conventionally conlateralred unpredictable using approaches developed for small rivers (LANGHORST; PAVELSKY, 2023; LATRUBESSE, 2008; SUIZU et al., 2022). These morphological changes identified from two-dimensional investigations provide indicators which, if interpreted correctly, can prove to be a valuable river management tool (BRIERLEY; FRYIRS, 2005; CARLING et al., 2018).

Bananal Island, located in central Brazil in the Araguaia River basin, is the largest fluvial island in the world (BORMA et al., 2009; DIAS et al., 2011; MENDES et al., 2015), featuring a complex network of channels generated during the Middle and Late Pleistocene by a multi-channel system (VALENTE; LATRUBESSE, 2012). Delineated by the Araguaia River on the left and the Javaés River on the right, the island is a unique system in the Cerrado biome in transition with the Amazon biome, which is still free from major direct alterations to the channel, such as the construction of dams (MARTINS et al., 2021; PELICICE et al., 2021). The current position of much of the Javaés River corresponds to an alluvial channel belt abandoned by the Araguaia River due to regional avulsion (IRION et al., 2016; VALENTE; LATRUBESSE, 2012).

In conjunction with the alluvial plain of the Araguaia and Javaés rivers, Bananal Island is considered the largest natural refuge for Cerrado fauna and one of the last remaining strongholds for biodiversity. It is regarded as an environmental frontier of the biome (LATRUBESSE et al., 2019; MARTINS et al., 2021; VALENTE; LATRUBESSE; FERREIRA, 2013). However, recent data indicates that more than half of the biome's vegetation cover has already been converted for anthropogenic use, primarily for agriculture and livestock (SOUZA et al., 2020). Environmental models suggest that impacts such as deforestation have a significant influence on processes in river systems like the Araguaia, affecting surface runoff and water recharge (COE et al., 2011, 2017; GOMES et al., 2021).

While some research has assessed morphological changes along the Araguaia River (BAYER et al., 2020; LATRUBESSE et al., 2009; SUIZU et al. 2022, 2023), so far, not much is known about the geomorphological dynamics of the Javaés River, on the other edge of Bananal Island. Consequently, understanding the morphological changes over time in the Javaés River is important for understanding the dynamics of the region's river system and identifying possible environmental impacts on local biodiversity. In addition, comparing these changes in the Araguaia and Javaés rivers will allow us to evaluate significant differences in river dynamics between the rivers surrounding Bananal Island. The objective of this study was to evaluate changes in the two-dimensional morphology of the Javaés River, using multi-temporal remote sensing images and trend analysis.

2. Materials and Methods

2.1. Study area

The area under analysis is located in a transition region between the Cerrado biome and the Amazon Forest, in the southeast of the Legal Amazon, in the state of Tocantins. The focus of the research is the lower reaches of the Javaés River (Figure 1), which is a reactivated palimpsest system resulting from successive detour (avulsions) of the Araguaia River during the Pleistocene (SUIZU; LATRUBESSE; BAYER, 2023; VALENTE; LATRUBESSE, 2012). Also known as the smaller branch of the Araguaia, the Javaés River delineates the entire right edge of Bananal Island, which is the largest river island in the world, draining an area of 53,000 km² of basin in the middle Araguaia River (MENDES et al., 2015).

The channel sections analyzed in the Javaés River begin at the confluence with its largest tributary, the Formoso River, at an altitude of 180 m. They present the best conditions for identifying depositional features in images from the LANDSAT satellite series, due to the width of the channel, which varies between 100 and 250 m. From this point, the river travels 118 km in a preferentially north-westerly direction until it bifurcates into two channels; the wider stretch flows into the Araguaia River 5 km after the bifurcation, at an altitude of 170 m. The adjacent branch has a 20 km stretch, called the Javaezinho River, and forms an island parallel to the Araguaia River in the Cantão State Park (PEC) (IBGE, 2007a).

This region is of great importance to environmental conservation, being surrounded by protected areas such as The Araguaia National Park (PARNA), the Canguçu Private Natural Heritage Reserve (RPPN), a scientific research base managed by the Federal University of Tocantins, the PEC and the Bananal Island/Cantão Sustainable Use Environmental Protection Area (APA) (Figure 1).

The climate in the Javaés River region traditionally is conlateralred humid, with moderate water deficiency, marked by a dry season, which varies between the months of May and September, and a rainy season, between September and April of the following year (SANTOS; CHEREM, 2021). Rainfall generation is influenced by the dynamics of the Intertropical and South Atlantic Convergence Zones that act over the southeastern portion of the Legal Amazon (NASCIMENTO; NOVAIS, 2020). The stretches of the Javaés River between PARNA and PEC (Figure 1) present the highest average annual rainfall rates in the entire Cerrado (between 1953 and 2,448 mm·year^{-1}). In the downstream to upstream direction of the Javaés River, the spatial distribution of precipitation gradually decreases, between 1003 and 1,161 mm·year^{-1} in the headwaters (CAMPOS; CHAVES, 2020; GOMES et al., 2022; GOMES; FERREIRA; LIMA, 2019).

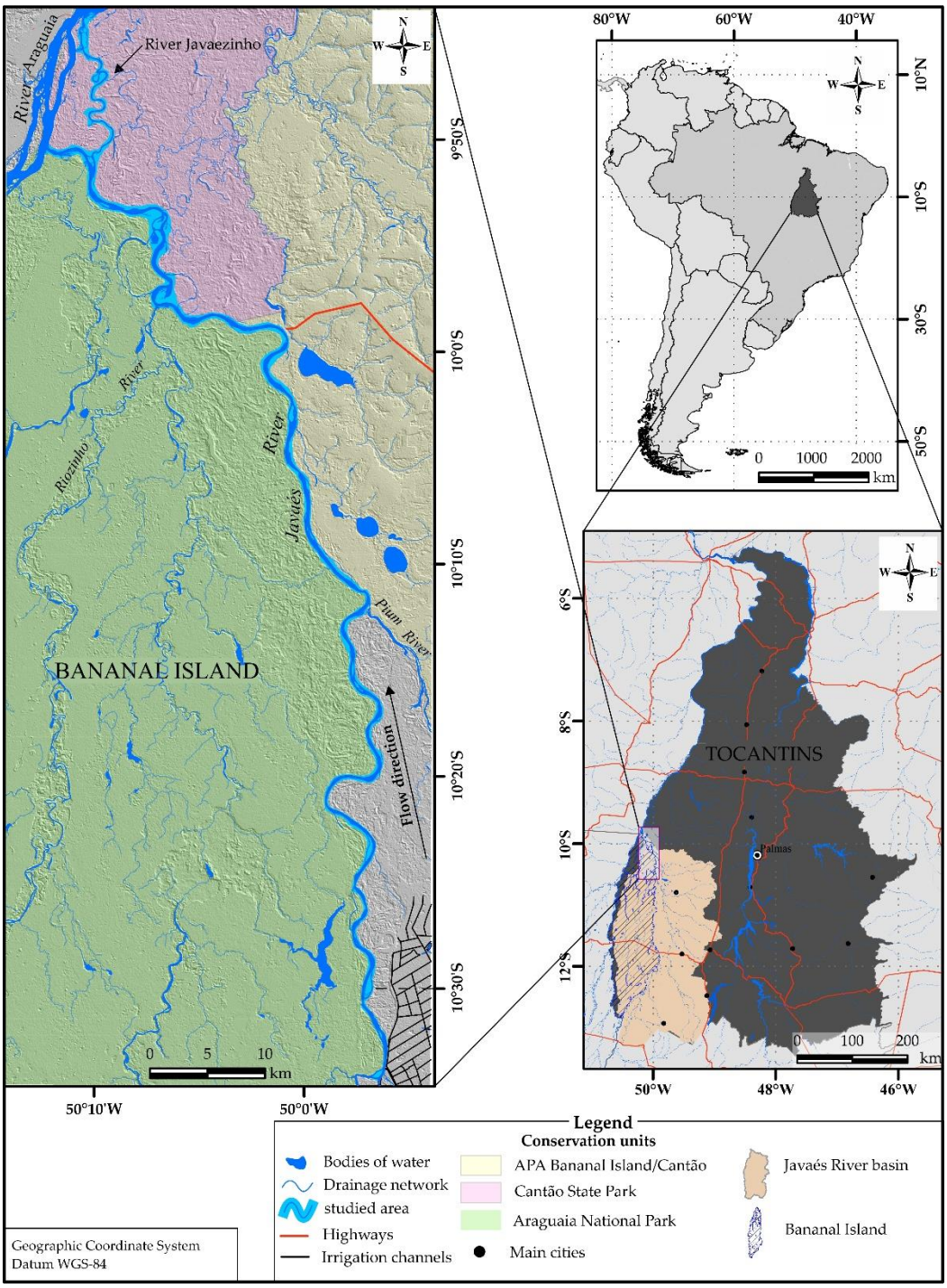

Figure 1. Location of the studied area. South America in light gray, Brazil in gray and the state of Tocantins in dark gray.

2.2. Mapping of fluvial features

In order to identify the fluvial depositional features, 4 topographic maps were used at a scale of 1:100,000 for the year 1968, vectorized and made available by the Brazilian Army's Geographic Service Directorate, and orbital data from the LANDSAT collection between 1985 and 2021 (Figure 2), which included the Landsat-4 and 5 satellites with the TM sensor, Landsat-7 with the ETM+ sensor, and Landsat-8 with the OLI sensor.

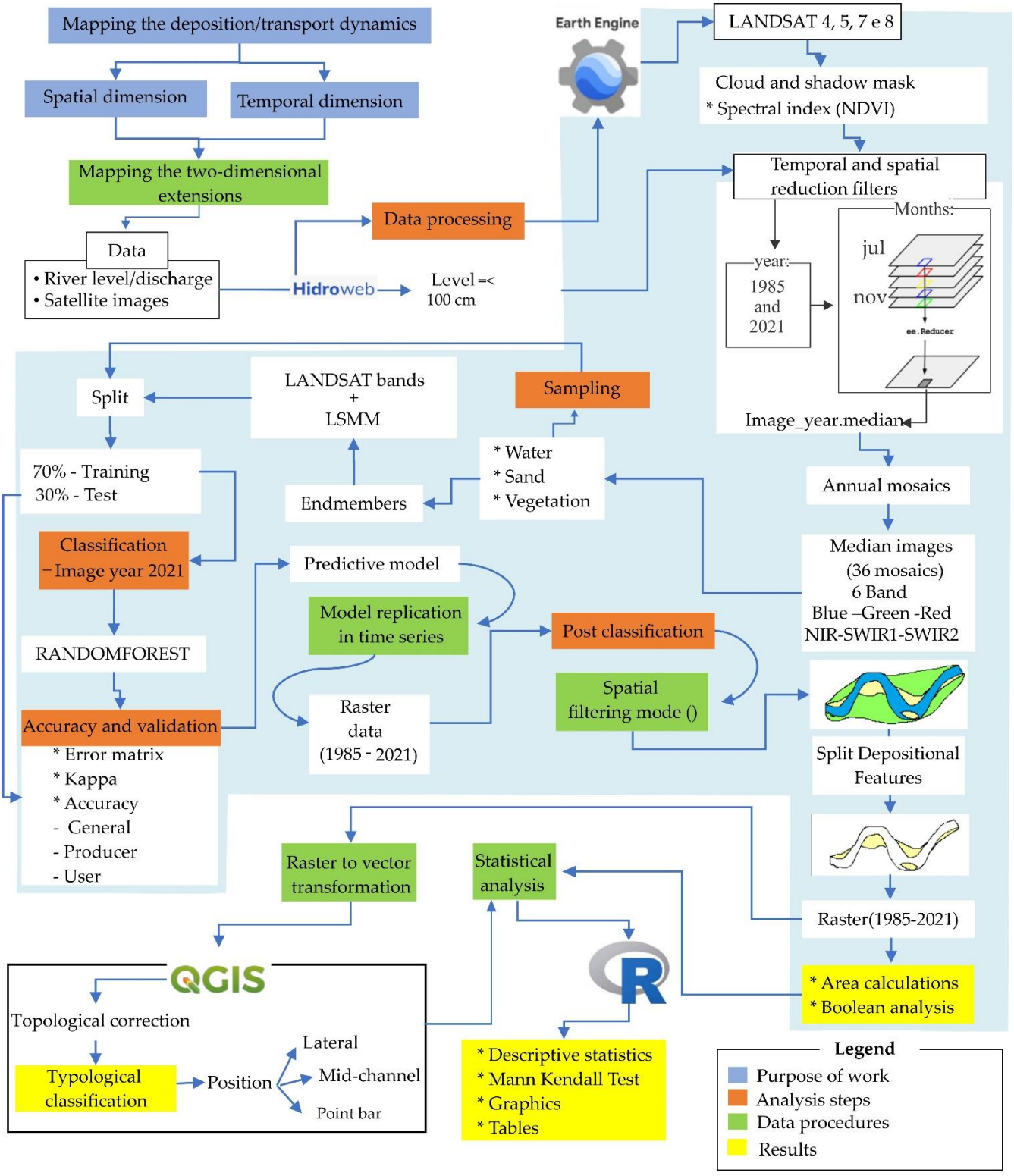

Figure 2. Workflow for time series identification.

The vectors of the topographic maps which correspond to the classes of bodies of water, sand bars and islands were extracted manually in the geographic information system (GIS) software QGIS (QGIS DEVELOPMENT TEAM, 2022). Therefore, a layer was created by merging the data, generating a file corresponding to the year 1968. For the orbital data, a Javascript programming language code was gradually developed on the Google Earth Engine (GEE) cloud spatial data processing platform (Figure 2), which offers an interactive cloud web interface (GORELICK et al., 2017). On the GEE platform, it was possible to access and use images from collection 2 of the LANDSAT satellite series, made available by the United States Geological Survey (USGS). In 2020, the USGS

finished reprocessing the raw data from the image series, applying new adjustments in the control points and georeferencing (PINTO; JING; LEIGH, 2020; WULDER et al., 2022). The Thematic Mapper (TM) and Enhanced Thematic Mapper Plus (ETM+) sensor images were then processed using the Landsat Ecosystem Disturbance Adaptive Processing System (LEDAPS) algorithm, while the Operational Terra Imager (OLI) sensor images were processed using the Land Surface Reflectance Code (LaSRC) algorithm, generating calibrated surface reflectance products, making cohesive harmonization between products possible.

In temporal comparative studies of fluvial processes in large rivers, sensor images with the smallest possible variation in hydrometric elevation are ideally used (e.g., PEIXOTO; NELSON; WITTMANN, 2009; FRAGAL; CREMON, 2012; ROZO; NOGUEIRA; CASTRO, 2014). However, for the study area in question, there was no available database with images from the Landsat series regularly spaced in time, whose scene coincided with the same hydrometric quota, or range of quota values close together. This was due to the temporal resolution of the LANDSAT series and scenes with cloud cover or cloud shadow.

In this context, we sought to work with images during the period in which the Javaés River had the lowest possible hydrometric level variability. A preliminary analysis of the hydrological level data from the Barreira da Cruz station on the Javaés River revealed that the period with the lowest level variability is between July and November (Figure 3). Santos and Cherem (2021) observed hydrological series and identified that, annually, in this same period of months, the Javaés River presents a dry phase with a flow of less than 100 $m^3 \cdot s^{-1}$ and less cloud cover.

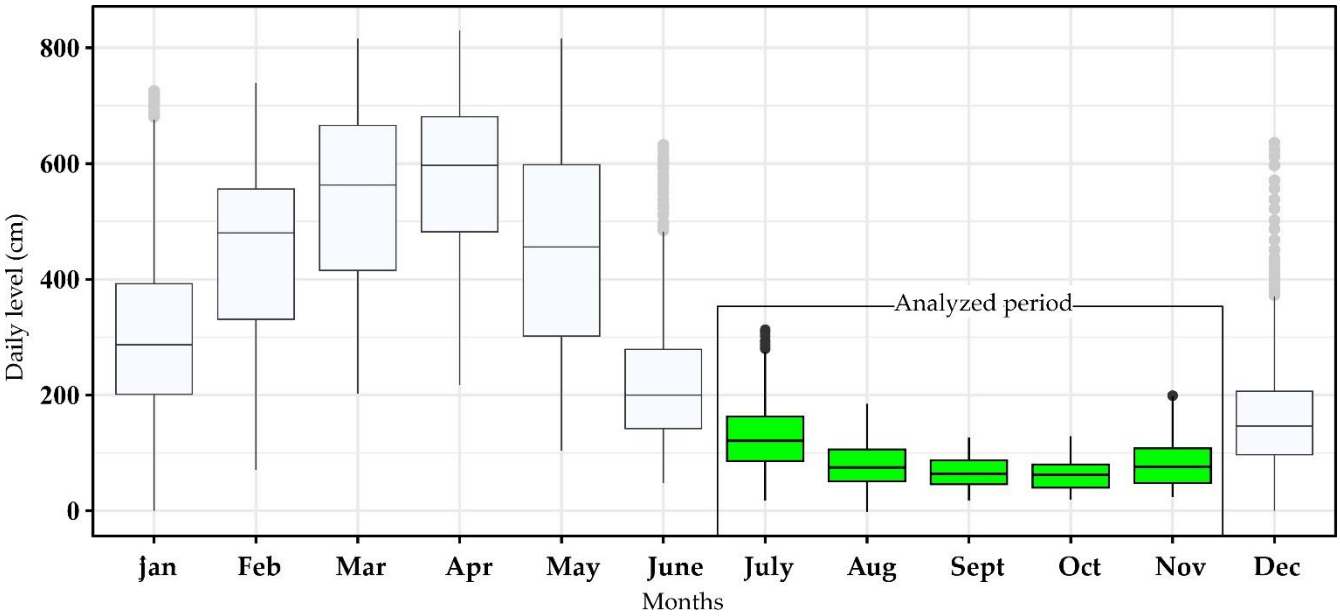

Figure 3. Boxplots with the historical series of average daily quota (in cm) from the Barreira da Cruz station. Data source: ANA (2023).

Thus, based on spatial and temporal filtering, it was selected 2,547 LANDSAT images generated between 1985 and 2021, restricting the search to the months of July and November. A pixel mask was applied in order to isolate clouds and shadows, using the pixel quality band developed by the USGS and aggregated in each set of scenes (LI et al., 2019). A median temporal reduction filter was applied to reduce the images, generating annual mosaics for each spectral band and year (TOBÓN-MARÍN; CAÑÓN BARRIGA, 2020).

Through this strategy, it was possible to acquire annual median images of the study area, with reduced cloud cover and at regular periods, as well as obtaining a baseline for comparison.

A supervised classification of the orbital images was used to map the depositional features, differentiating these targets from the sand bar, water, and vegetation classes. For this, the Random Forest algorithm was used, which uses an approach that combines several random decision trees to obtain the best accuracy in dividing between classes, generating a predictive model with the best results using an ensemble machine learning approach (BORRA; THANKI; DEY, 2019; BREIMAN, 2001).

The multispectral bands of the LANDSAT series in the visible (BLUE, GREEN and RED) and infrared (NIR, SWIR1 and SWIR2) ranges and the normalized difference vegetation index (NDVI) were used for each annual

mosaic of images generated. In addition, based on the Linear Spectral Mixture Model (LSMM), it was possible to obtain fractional images for each year of the endmembers: sand, water, and vegetation (SHIMABUKURO; DUTRA; ARAI, 2020; SHIMABUKURO; SMITH, 1991). The endmembers were selected by visual interpretation when defining pure pixels for the application of LSMM using the unmix function in GEE.

In the classification sampling process, 1,047 points were selected from the images according to the three specified classes (sand bar, water, vegetation). The samples were divided into two groups, 70% of which were used for training and 30% for testing (validation with samples independent of training) (BORRA; THANKI; DEY, 2019; NGUYEN et al., 2021).

The results of the images classified in matrix format were post-processed with a 3x3 median filter and then converted into polygon-type vectors on the GEE platform. The data was then entered into QGIS to clean the polygons and correct the topology manually, reducing inconsistencies such as overlaps and gaps between borders. Specific years were selected for vector detailing, 1968 being related to the vectors of the topographic maps, 1985, 1990, 1995, 2000, 2005, 2010, 2015 and 2021 derived from the classification of the LANDSAT mosaics.

2.3. Types of depositional features

Geomorphological definitions of macroforms of riverbed relief were used, primarily considering their position in the riverbed and the processes of formation (CHARLTON, 2008; CHRISTOFOLETTI, 1981; STEVAUX; LATRUBESSE, 2017), observing the proposals adapted for mapping tropical rivers such as the Araguaia (MORAIS, 2006; SUIZU et al., 2022). Based on these references, five types have been identified in the study area: point bar (Figure 4A), lateral bar (Figure 4B), tributary confluence bar (channel junction bar) (Figure 4C), central bar (Figure 4D), islands and added bars (Figure 4E).

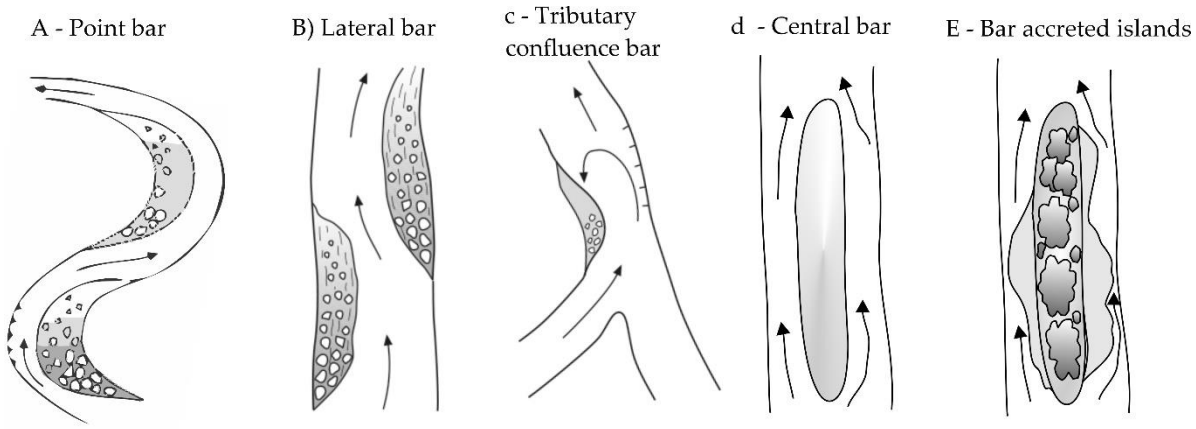

Figure 4. Representations of mapped bar patterns and river islands. Source: Adapted from Brierley and Fryirs (2005) and Suizu et al. (2022). Diagrams available at: https://riverstyles.com/geomorphic-unit-quick-reference-guide/page/2/E

The islands have also been mapped, but they were identified manually, by individualizing polygons associated with the presence of vegetation between river channels (Figure 4), with specific adjustments between the boundaries between bodies of water and sand bars. Figure 5 exemplifies this identification and the typologies observed in the Javaés River, based on LSMM images.

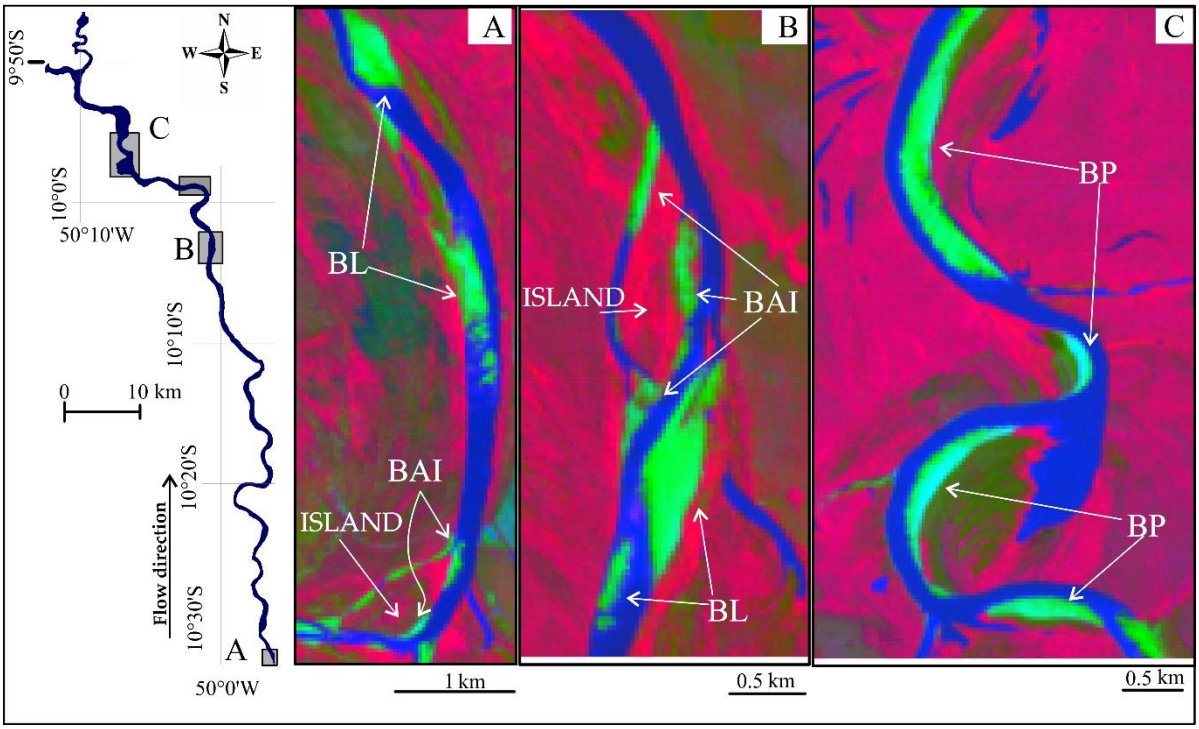

Figure 5. Location of the control area in the mapping of sand bars and islands in the Javaés River. The symbols correspond to: BL - Lateral Bar; BAI - Bars added to islands; BP - Bar at Point; BJ - Bar at Junction of channels. LSMM image in color composition: R (vegetation fraction image), G (sand bars fraction image), and B (water fraction image). The bodies of water appear in blue, the sand bars (in light green) and the vegetation in varying shades, magenta for the tree pattern and olive green for the shrub pattern.

2.4. Time series and trend analyses

The time series was analyzed for the entire area studied with continuous data between 1985 and 2021, using statistical tests, graphical analysis, and map algebra. The QGIS software was used to define 14 5 km-long segments along the channel, named A (upstream) to N (downstream), calculating the area, azimuthal orientation and sinuosity for each section. Descriptive statistical analysis was performed using R statistical software (R CORE TEAM, 2020), generating tables and graphs.

Through the *Trend* package, the function *mk.test* was used, which applies the non-parametric Mann Kendall test (MCLEOD; MCLEOD, 2015), commonly used to identify the presence or absence of a trend in time series (FIENER; NEUHAUS; BOTSCHEK, 2013; SANG; WANG; LIU, 2014; SANTOS; CHEREM, 2021), and the Sen` Slope estimator, which quantifies the magnitude of these changes (HAGHTALAB et al., 2020; MU; JONES, 2022; SEN, 1968). The moving average of the time series for 3 consecutive years was also calculated to identify sub-trends. Also in the R software, the relationship between the development of the area of sand bars and water bodies was calculated based on a simple linear regression test.

The GEE also analyzed the spatial evolution of bodies of water and sedimentation over time and between stretches, using simple algebra of the rasters generated in the classification. This process involved considering the pixel position differences between two periods, with quantification of the areas removed, stable or added (GUIMARÃES; NARVAES; GALO, 2017). For the 14 defined stretches, the sediment balance was analyzed, as well as the statistical trend analysis (MK) for the area of water bodies and sand bars.

3. Results

3.1 Multi-temporal analysis of the distribution and trends of sand bars and water bodies

In identifying targets, the model trained with the Random Forest classifier showed overall accuracy and a Kappa index of 0.99. The values for the area of the classifications of channel water bodies and sand bars were organized into time series as shown in Figure 6. Between 1985 and 2021, the bars varied with a minimum area of

9.5 km² in 1995 and a maximum of 20.8 km² in 2017. The water bodies showed a range of 16.8 km², with a minimum area of 21.7 km² in 2016 and a maximum of 38.6 km² in 1985. Sand bars increased in area between 1985 and 2021 by 57% (6.5 km²), while the area of water bodies decreased by 39% (15.2 km²).

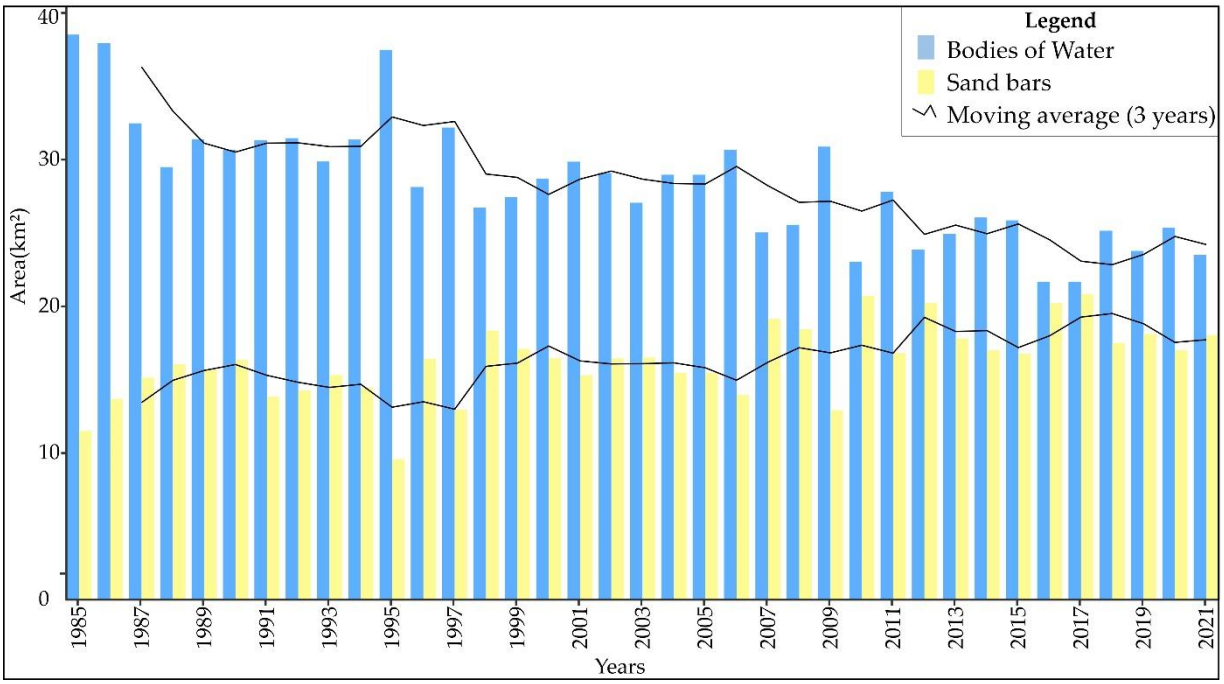

Figure 6. Sum of annual mapped areas of sand bars and bodies of water between 1985 and 2021 in the lower reaches of the Javaés River.

The Mann Kendall (MK) non-parametric test applied to the data on sand bars indicated a statistically significant trend in the time series (t=0.48, p-value<0.05), with an increase in the area of sand bars (sen's slope = 0.12 km²·year^{-1}, p-value<0.05). The same analysis applied to the water mass series also indicates the presence of a trend (tau = -0.63, p-value < 0.05), but with a reduction in area (sen's slope = -0.28 km²·year^{-1}, p-value < 0.05). The linear regression test indicated a significant relationship with a positive correlation between the area of the sand bars and the area of the water bodies, indicating that the increase in deposition rates may be conditioned by the reduction in the area of the water bodies (R^2= 0.84, p-value= 0.01).

The values of the moving average of area adjusted for 3-year periods made it possible to identify oscillatory phases in the data, with gradual increases and decreases that indicate sub-trends in both groups (Figure 6). The sand bars increased by 40% between 1985 and 1990, reaching a peak in 1990 and then a phase of reduction which culminated in the lowest point in the historical series in 1995. Depositional features resumed their growth between 1997 and 2000, remaining at a level of around 15 km² until a drop in 2006 (14 km²). Between 2006 and 2011, the area of bars increased to around 18 km², followed by a reduction in area until 2015. In 2016 and 2017, there was an increase in area of over 20 km² again, with a reduction and stabilization at around 18.5 km².

The bodies of water showed milder fluctuations in annual area, alternating between sequences of area reduction, peaks, and periods of stability. In 1985 and 1986, the values were the highest in the series, followed by a 24% reduction in 1988. A plateau was maintained until 1995, with values between 30 and 32 km² in the following years, reaching a peak in 1995 (37.5 km²), with an isolated rise to a level similar to 1985. From 1996 until 2005, there was a phase of stability. From 2006 onwards, the areas of water bodies fell by 7.1 km² (-23%) until 2021. The years 2015 and 2016 represent a period of reduced area in the water bodies of the channel, followed by a resumption in the expansion in area of the sand bars. When analyzing the data between 2015 and 2021, it can be seen that the area of sand bars increased by 7.6%, while the area of water decreased by 11.5%.

Map algebra between regular periods (Table 1) indicated that the water bodies had the greatest increase in channel area between 1990 and 1995 (10 km²) at a rate of 2.5 km²·year^{-1}. Proportionately, there was greater mobility of the sand bars in this same period (8.1 km²), at a rate of 1.7 km²·year^{-1}. Subsequently, between 1995 and 2000 there was a reduction in the area of water bodies in a similar proportion to the previous period, with an increase

in the deposition of bars at a rate of 1.5 $km^2 \cdot year^{-1}$. Between 1985 and 2000, the stable areas had regular values, with a progressive reduction in later periods. The sand bars showed oscillating values between the periods in the rates of mobility and accretion of areas and a gradual increase in the areas of stability.

Table 1. Results of the Boolean analysis of the area balance between periods on the Javaés River.

	A - Area of bodies of water			B - Area of sand bars		
Periods	Accretion	Stable	Mobility	Accretion	Stable	Mobility
1985-1990	2.4	27.6	-7.2	6.1	10.2	-1.3
1990-1995	10	27.4	-2.5	1.3	8.3	-8.1
1995-2000	1.3	27.4	-10.0	8.0	8.5	-1.1
2000-2005	2.3	26.7	-2.0	1.7	13.8	-2.7
2005-2010	0.5	22.5	-6.5	5.8	14.9	-0.6
2010-2015	3.9	22.0	-1.1	0.9	15.9	-4.8
2015-2021	1.2	22.3	-3.6	3.1	14.9	-1.8

3.2 Sectional analysis of sediment balance and trends in sand bars and water bodies areas

The 14 defined stretches are shown in Figure 7A. Section A is a channel generated from the confluence of the Javaés River with the Formoso River (Figure 7A), its main tributary which holds most of the upstream channels. Along with section B, this sector has the following characteristics: a unitary channel with alternating lateralbars, a recurrence of multichannel segments with large islands (Figure 7A), an average width of 144 m, low sinuosity and NNW and N direction control. The sinuosity increases in stretches C and D, with an average width of between 124 m and 137 m, with alternations in the orientation of the meandering curves between NE and NW. The F section shifts direction after receiving flow from the Pium River on the right bank, with the Javaés River reorienting to NNW until the H section. The sections between I and L show the Javaés River shifting to W, alternating direction with NW segments until the main confluence with the Araguaia River. The average width of the stretches in this section varied from 139 m in section I, with sinuous characteristics and deposition in bars at the point, to 208 m in section K, which concentrates islands and lakes integrated into the ebb bed. The sinuosity is greater than 1.5 up to the bifurcation of the main arm. The sinuosity is greater than 1.5 up to the bifurcation of the main branch. The M and N stretches represent this secondary trunk, the Javaezinho River, a channel with an active regional avulsion characteristic, oriented perpendicular to the Araguaia River (varying in direction between NE and NW); both have the highest sinuosity rates among the stretches (1.8) and the lowest width rates (76 and 101 m).

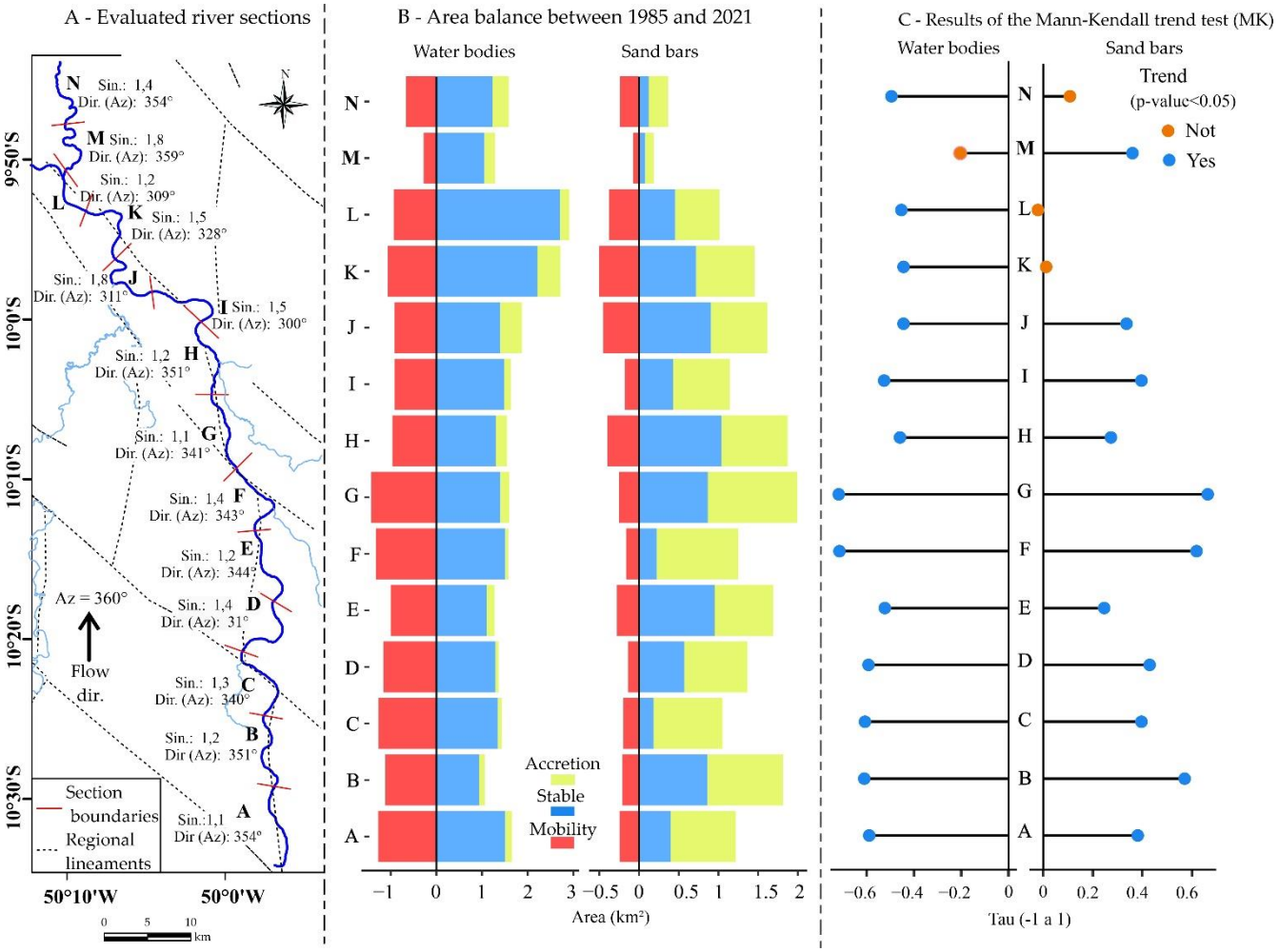

Figure 7. Segments analyzed in the study area and trends over time. (A) Location of the defined segments for the study area with orientation (Az) and sinuosity (Sin) and regional lineaments (IBGE, 2008). (B) Area balance: Accretion, stability, and mobility of water masses and sand bars. (C) Results per segment from Mann Kendall trend tests (MK).

The Boolean analysis of the difference in area between 1985 and 2021 reinforced the identification of changes in the area balance of the Javaés River. The phases in the areas of the bodies of water showed a reduction of 14.2 km² (Figure 7B), an increase of 3 km² and a stable area of 20 km². Each section lost approximately 1.4 km² of water mass on average, with the highest values in sections G (1.4 km²), F (1.3 km²) and A (1.3 km²). The accretion of new channel areas was progressive between the sections from upstream to downstream, ranging from 0.06 km² (section F) to 0.5 km² (section K). The stable areas were higher in the downstream stretches, in sections directly associated with the presence of large islands and multi-channel stretches, such as L (2.7 km²), K (2.2 km²) and A (1.5 km²). The sand bars showed an increase of 10 km², a decrease of 3.7 km², and a stable area of 7.7 km². In 37 years, sectors G and F have added the most areas of sand bars. Sectors A, B, C, I, J, K, M and N have a higher accretion rate than the stable areas. Sector H also stands out with the largest stable bar area (1.03 km²).

The results of the MK test on the temporal distribution of water bodies indicated the presence of a pattern (p-value < 0.05), with a negative slope in 13 mapped stretches (Figure 7C). The MK test of the temporal distribution of the areas of sand bars identified the presence of a statistically significant trend in 11 of the 14 segments (p-value < 0.05), with a positive variation in the statistical indicators of the tau index between 0.25 (stretch E) and 0.67 (stretch G). The results of the sen's slope index confirm the dominance of the positive slope with values varying between 0.001 and 0.02 (p-value < 0.05). Sections F and G, in the central section, show a greater difference in accumulation rates in all years when compared to the other sections and also the highest values of the tau and sen's slope indices, indicating that these zones in the river have shown a greater capacity for accumulating

sediment. Between sectors H and J, the tau index values are set at similar levels to the upstream stretches between A and D.

The MK test results for sections L, K and N all indicated stability in the deposition balance in this section. The analysis of discrepancies between periods have indicated that the area lost to sedimentation is proportional to the area generated in this sector. Even though the results for the N stretch showed no trend towards changes in the annual sediment input, morphological changes were observed in the mapping sequences between 1985 and 1990, with the occurrence of a meander cut, the formation of islands and secondary connections to the Araguaia River and a reduction in the area of the mouth. The visual analysis of the LSMM also shows secondary vegetation (VS) in shades of olive green (Figure 8), colonizing abandoned channels and depositional features.

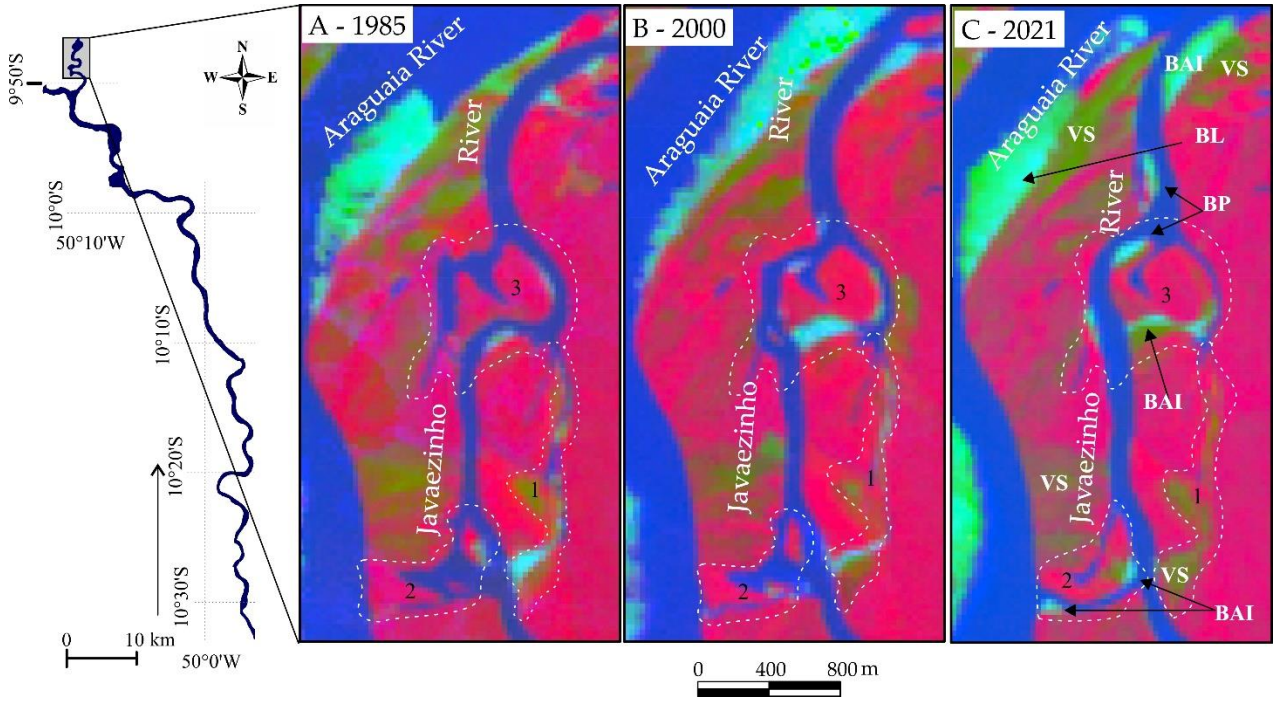

Figure 8. Color composite image R (vegetation fraction image), G (sand bars fraction image), B (water fraction image) of the LSMM, with indications of changes in the channel morphology of the N section and at the mouth of the Javaezinho River next to the Araguaia River. Highlighted (dotted lines), secondary vegetation (VS), incorporating the abandoned channel into the floodplain (1), shortening of the sinuous curve with the formation of a paleochannel (2); installation of a borehole, connecting the two rivers (2); Island welding (3).

3.3. Classification and morphometric analysis of depositional features and islands

The analysis of the data in Table 2 for the lower reaches of the Javaés River reveals a trend for the frequency and area of features to increase over the years selected for vectorization. It is interesting to highlight that the number of features shows an increase of 107% between 1968 and 2021, at an annual rate of 2%, which is a non-linear increase. The most significant increase in frequency took place between 1968 and 1985 of 110%, at an average annual rate of 6.4%. On the other hand, between 1995 and 1990 there was less growth (4.07%) in the frequency of features, while between 2000 and 2005 there was a reduction of -4.8%.

Regarding the temporal distribution of the frequency of sand bars by feature type, in 1968 the predominant group was point bar, representing 41% of the total, followed by the lateral bar (14) and Islands (13) groups, respectively 21% and 19% of the features. These three groups maintain their dominance among the typologies mapped in the Javaés River, representing 84% of the total mapped features in 2021. This percentage of dominance has changed with the gradual reduction of islands and a significant increase in lateral bars.

Between 1968 and 1985, the number of point bars increased by 75%. However, in the following periods, it showed variable rates, with a sequential drop between 1985 and 1990 (-14%) and another between 1990 and 1985 (-7%), followed by an increase between 1995 and 2000 (23%). Between 1968 and 2021, lateral bars presented the largest absolute increase among the groups, with an increase of 39 bars. Between 1985 and 2021, this group

maintained an upward trend, with a relative difference of 179%. Between 1968 and 1985, the islands showed a significant increase (107%), although they showed a downward trend until 2021.

Table 2. Frequency of types of sand bars and islands in the lower reaches of the Javaés River. NA = no record.

Year	Bars added to the islands		Central bar		Bar at junction of channels		Point bar		Lateral bar		Islands		Total	
	Freq.	Area (km²)	Freq.	Area (km²)	Freq.	Area (km²)	Freq.	Area (km²)	Freq.	Area (km²)	Freq.	Area (km²)	Freq.	Area (km²)
1968	10	1.3	1	0.04	2	0.06	28	7.9	14	2.1	13	3.7	68	15
1985	18	1.3	6	0.05	6	0.17	49	8.2	38	2	26	2.7	143	14.4
1990	27	1.8	9	0.28	8	0.17	42	10.4	40	3.8	23	2.4	149	19.0
1995	22	1.1	6	0.10	9	0.16	39	6.5	41	1.5	27	3.0	144	12.4
2000	26	1.9	5	0.12	8	0.16	48	11.1	41	3.2	23	3.3	151	19.8
2005	31	1.9	NA	NA	9	0.24	40	10.3	41	2.9	23	2.5	144	17.9
2010	23	2.5	5	0.03	13	0.34	52	14	45	3.9	22	3.2	160	24
2015	16	1.3	1	0.01	7	0.19	44	11.3	37	3.0	20	2.2	125	18
2021	13	1.2	4	0.02	6	0.28	48	13.1	53	3.9	17	2.6	141	21.1

From 1985 onwards, the frequency of bars on a pier behaved similarly to the total frequency of mapped features, as did the lateral bar group, which showed a continuous increase in features until 2021 (Table 2). In contrast, the islands and bars added to the islands showed reductions over each period, with the highest frequency in 1995 (27) reaching 17 features in 2021. Bars added to islands accounted for 14% of features in 1968, rising to 31 features in 2005. The central bar showed a low frequency throughout the series, with no record in 2005. The bar at the junction showed a similar trend to the group of added bars, with a gradual increase in frequency up to a peak in 2010 and a reduction of 46% in 2015.

Table 2 also shows the total area per year, incorporating the measurements of the charted islands. The vectorized features show an asymmetrical distribution of area, with an average of 0.13 km², a median of 0.05 km², and a range varying from 4,352 m² to 1.2 km². In absolute terms, the bars in point add up to a greater percentage of area over the time series, following the oscillating trend of a more significant drop in 1995. This group has the highest means and medians, 0.2 km² and 0.1 km² respectively, followed by the Island group (0.1 km² and 0.03 km²). The central bars showed the greatest median expansion in area between 1968 and 1995, with a drop between 1990 and 2021 (0.26 km²). Between 1990 and 1995 the bars at the point, lateral bars and central bars reduced their areas by -38%, -60% and -61% respectively, and only the Island group showed no reduction (22%). The period between 1995 and 2000 was the most positive in terms of area growth, driven by the point bars (Table 1). Between 2010 and 2015 there was a predominant reduction in area, especially in the central bars (-81%).

The bars at the junction of channels indicate an increase in area between 2015 and 2021, which suggests greater dynamics between connections of connected systems such as the mouths of the Formoso (Figure 5), Pium and Riozinho rivers and bifurcations in sectors such as the Javaezinho river channel.

When conlateralring the central trend indicators, the central bar group has the smallest area range, with a unimodal concentration around the median of 616 m² (Figure 9). The reduction in the number of central bars directly affected the area of this group between 2015 and 2021. Apart from the central bars and the bars at the junction, the other area values per group indicate a downward trend between 1985 and 1995, followed by an increase in 2000 and an upward trend until 2021. The median area of the added bars was reduced between 1968 and 1995, with values oscillating between 0.01 km² and 0.11 km². Despite the reduction in quantity and total area, there was a median increase in the size of these features (Figure 9). Between 1985 and 2021, the average size of the islands fluctuated between 0.10 km² and 0.15 km² and the maximum between 0.5 and 0.6 km². The area of the

islands within the quartile was close to or less than 0.01 km², while the median area oscillated without a linear trend, with greater dispersion and a trend to increase in 2021.

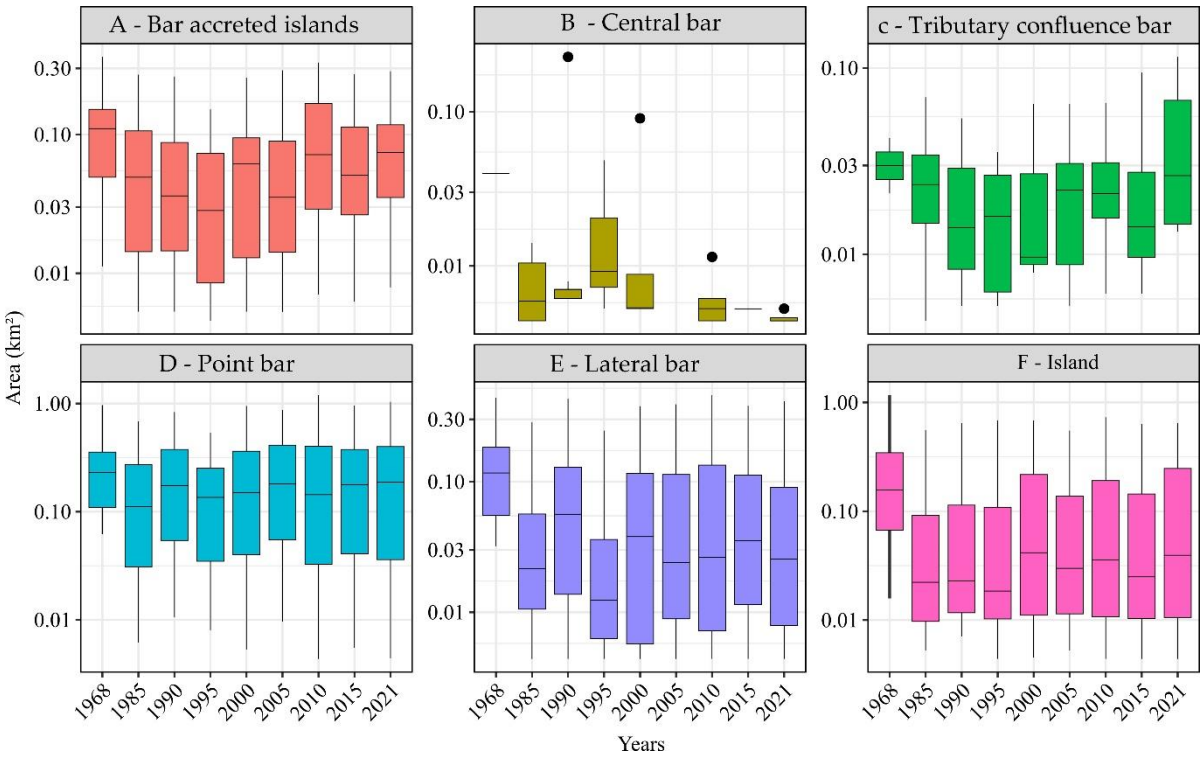

Figure 9. Area of features mapped in the Javaés River according to groups of: (A) bars added to islands (B) central bar; (C) bar at junction of channels, (D) point bar, (E) lateral bar, (F) islands.

4. Discussion

4.1 Variables that control and influence channel dynamics

Mapping the Javaés River over 53 years has revealed significant changes in the morphosedimentary balance, with a reduction in the area of water bodies and an increase in sediment input. It is essential to understand the internal and external factors that condition the formation of macroforms in order to understand the adjustments observed (FRYIRS; BRIERLEY, 2012). When these factors are in balance, rivers tend to have sedimentation rates and river discharge in a state of equilibrium (MAGALHÃES JÚNIOR; BARROS, 2020; SEAR; NEWSON, 2010). However, changes in the liquid discharge, cohesion of the banks, transversal increase of the channel and blockages in the beds can unbalance the processes of flow and deposition (STEVAUX; LATRUBESSE, 2017).

Studies on the climate dynamics of the Cerrado Biome and the southeastern transition region between the Amazon and the Cerrado have shown changes in the distribution and frequency of rainfall (AGUDELO et al., 2019; ARVOR et al., 2017; FUNATSU et al., 2021; NETO et al., 2021; SANTOS; LUCIO; SILVA, 2015; HOFMANN et al., 2023). Analysis of data from meteorological stations (ANA) and interpolation grids (CHIRPS; PERSIANN-CDR) between 1977 and 2010 indicated that the anomalies of the Atlantic and Pacific oceans (El Niño and La Nina) have a significant influence on the rainfall regime, with a general downward trend in monthly averages in the Cerrado (-8.4%), highlighting a reduction in the series until 1998, followed by stability until 2010 (CAMPOS; CHAVES, 2020). Observations between 1977 and 2006 (MARCUZZO; ROMERO, 2013) and between 1982 and 2019 (GOMES et al. 2022) have shown that these phenomenological anomalies have a moderate influence on the spatio-temporal variability of rainfall in the region.

Gomes et al. (2019; 2022) pointed out that the Araguaia River basin shows high annual variability in precipitation and average flow along its course, with flood peaks and prolonged droughts associated with the intensity of El Niño and La Nina episodes. Arvor et al. (2017) identified, using data from the PERSIANN-CDR project, a trend towards a shorter rainy season in the southern portion of the legal Amazon in the Araguaia basin between 1983 and 2014. Highlab et al. (2020) confirmed this trend by analyzing daily data from the CHIRPS

program between 1982 and 2018, also indicating that the same region has the highest number of dry days, and greater trends towards extremes of drought.

Marengo et al. (2022) has identified negative trends in precipitation dynamics in the transition zone between biomes in the Eastern Amazon and Cerrado, associated with longer periods of drought and increased water stress. Data from Bettiol (2021) also showed a negative trend in precipitation in a large part of the Javaés River basin and on Bananal Island between 2000 and 2019, mainly with episodes of drought in December.

This research is related to studies on the Javaés River by Santos and Cherem (2021), who evaluated the precipitation and flow of this river in relation to the average monthly behavior of the Araguaia River between 1984 and 2020. This research identified trends of reduction in accumulated monthly precipitation in both rivers between January and June, corroborating a regional behavior of intensification of dry periods, with a reduction in flow in the months of June, July, August, October and November, the period analyzed in the bar mapping.

4.2 Influences of anthropogenic activities on river systems

South America has undergone an intense conversion of natural areas into anthropogenic environments, totaling around 60% between 1985 and 2020 (ZALLES et al., 2021). This region has some of the largest river basins in the world, which drain different geomorphological environments and are home to great environmental diversity and endemism (LATRUBESSE; STEVAUX; SINHA, 2005; PELICICE et al., 2021). In the center-west of Brazil, in contact with the southwest of the legal Amazon, the dynamics of land use and occupation have generated significant impacts on river systems. Factors such as deforestation (BAYER et al., 2020; CASTRO, 2005; HUNKE et al., 2015; SANTANA et al., 2007), pasture expansion, extensive agriculture and the construction of dams have been identified as environmental stressors in this region (LATRUBESSE et al., 2019; GOMES et al., 2021; PELICICE et al., 2021; MARTINS et al., 2021).

In the Araguaia River basin, mapping has quantified geomorphological dynamics and identified associations between anthropogenic activities and changes in the river channel (BAYER, 2002; FERREIRA et al., 2016; LATRUBESSE et al., 2009; LATRUBESSE; STEVAUX, 2002; MORAIS, 2006). Between 1960 and 2000, there was an increase in sediment input related to deforestation in the basin, leading to a regime of channel interlacing and an increase in islands (MORAIS, 2006; FERREIRA et al., 2008; LATRUBESSE et al., 2009; COE et al., 2011; BAYER et al., 2020). Suizu et al. (2022; 2023) highlighted a change in this trend of channel interlacing, indicating that between 2001 and 2018 there was a reduction in sand bars and an increase in vegetated islands.

The changes on the west bank of the Javaés River are the result of the country's economic dynamics, making the region strategically important for the modernization of agriculture (RADAMBRASIL, 1981; SILVA, 2000). Major irrigation poles were implemented by government programs, such as the Japanese-Brazilian Cooperation Program for the Development of the Cerrados (PRODECER), the Southwest Development Program of the State of Tocantins (Prodoeste), and the inclusion of the area in the MATOPIBA agro-industrial interest region (ALVES, 2020; BLANCO et al., 2022; MORAIS; JÚNIOR; MENEZES MARTINS, 2017). These economic factors have made it possible to expand the production of agricultural commodities over time, controlling the dynamics of natural flooding and the flow of rivers in the region. The construction of dams, artificial channels and intensive collection of water for irrigation during the dry season have made intense cultivation possible, but have also resulted in a water deficit, reduced longitudinal and lateral connectivity between the region's plains and rivers (SANTOS; CHEREM, 2021).

Water shortages in the region have been reported by the media, with agricultural activities intensifying during annual droughts, raising the possibility that intense agricultural use during critical periods could reduce water availability and cause irreversible changes in the river systems of the Bananal Island region (FLEISCHMANN et al., 2017). Analyses of water use in the tributaries of the Javaés River indicate that 72% of irrigation enterprises use water from the system during the period of greatest hydrological and climatic criticality (FAGUNDES, 2021).

Historical land use and land cover mapping data from the MAPBIOMAS project (collection 7) (SOUZA et al., 2020) revealed the environmental changes in the Javaés River region. A consultation of the data from this database is shown in the graphs in Figure 10, with an area cut out for the zone of influence of the Javaés River (29,775 km²) defined by Santos and Cherem (2021). The deforested area declined at the end of the 1980s and increased significantly in the 1990s, peaking in 2004 (Figure 10A). Secondary deforestation continued to grow until 2013, while total deforestation peaked in 2013, followed by a downward trend in recent years. APA Ilha do Bananal was

identified as the conservation unit in the region with the highest increase in deforestation over the last decade in Brazil (BLANCO et al., 2022).

The historical series of wetlands between the years 1985 and 2021 (Figure 10B) shows variations, with a downward trend, phases of stability and an increase in 2011. These areas correspond to floodplains with obstructed flow, or with poor drainage (BRAZIL, 1981; IBGE, 2007a; IRON et al., 2016). During the rainy season, they are seasonally flooded or saturated (SANTOS; CHEREM, 2021) and they feature herbaceous phytophysiognomies associated with wetlands and tree vegetation associated with the Cerrado Park and Palm Grove (DURIGAN et al., 2022). The ipucas are typical features among these wetlands of the mid-Araguaia, and have a distinct topography from the floodplains with a depressed position and semicircular shape (MANCHOLA; MORAIS, 2023). The ipucas are occupied by forest fragments of hydrophilous and hygrophilous herbaceous vegetation (MARTINS et al., 2006). They concentrate the surplus from natural flooding and can connect the flows of the plains with intermittent river systems or the surface with the subsurface through sinkholes (IRON et al., 2016).

According to Figures 10A and 10C, the expansion of irrigation areas is due to the progressive reduction of wetlands. Between 1985 and 2020, irrigation areas increased 13-fold, with an average annual growth rate of 6.64%. This expansion has two distinct trends: an increase until 2000, with a peak of 347 km², followed by a drop in 2002 and a new increase from 2003 onwards, reaching a new peak in 2019, with 877 km². In addition, the average annual flow at the Barreira da Cruz station showed a downward trend over the years, despite annual fluctuations. This reduction can be attributed to the increase in the irrigation area, which affects the availability of water in the rivers, but it can also be the result of changes in rainfall dynamics and increased sediment input that reduces the depth of the channel.

The years 2016 and 2017 showed the lowest average water flow indicators throughout the historical series of the Javaés River, with a reduction in the area of water bodies and an increase in the area of sedimentation. The hydrological drought was worsened by increased demand during drought periods, leading to the temporary suspension of water abstraction from tributaries and the Javaés River, and the installation of the first real-time monitoring system for water abstraction from a river for irrigation in Brazil (FLEISCHMANN et al., 2017). Hydrological analyses indicate that irrigation systems in the region have a significant impact on the water balance of the tributaries of the Javaés River and show that the collection and distribution systems in the plains are inefficient, resulting in wasted water and greater pressure on the rivers (VOLKEN et al., 2022). These models suggest that a 35% reduction in the volume of water used for crops would be necessary to avoid an increase in intermittency due to human activities.

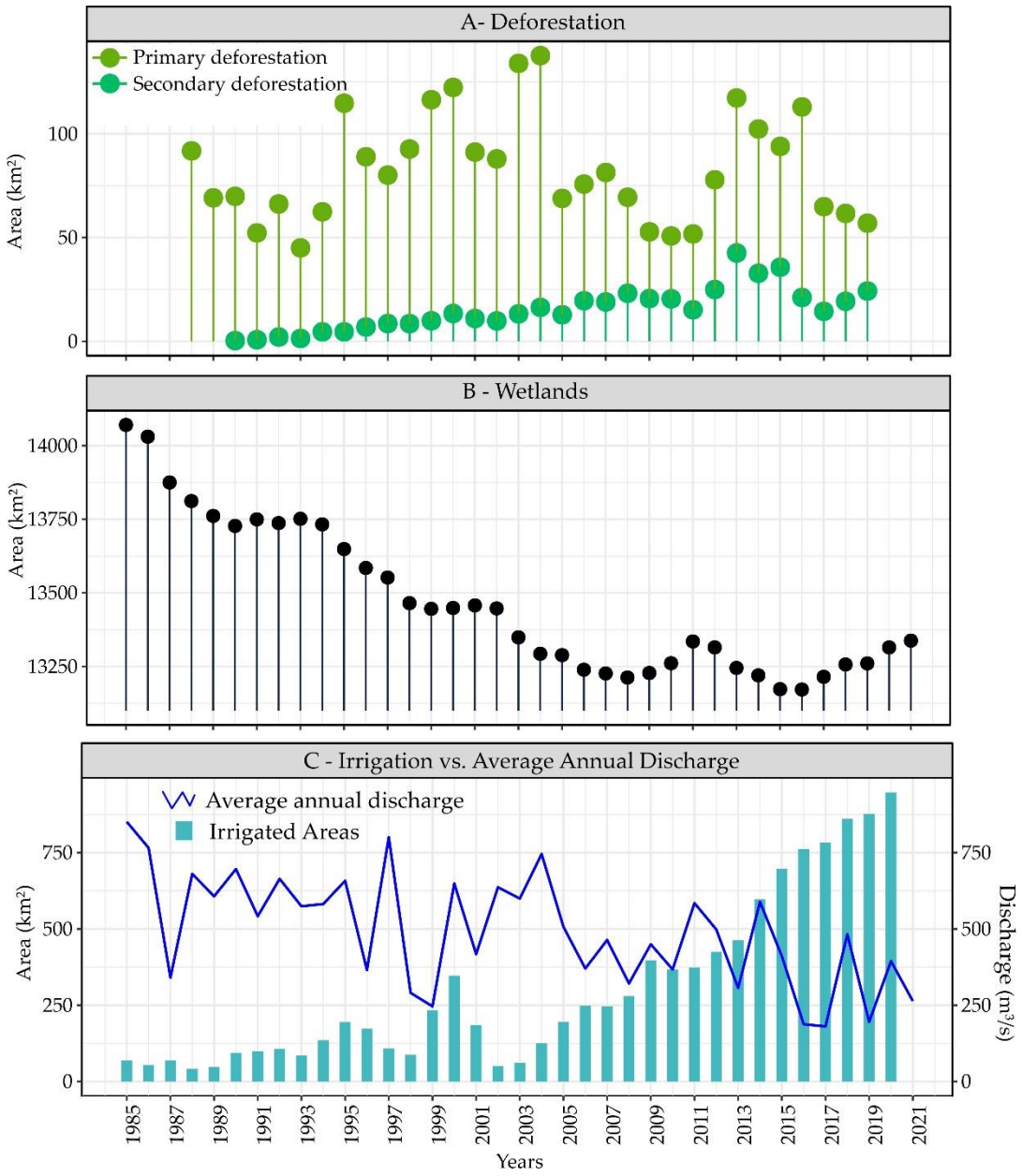

Figure 10. Historical series with land use and cover classes in the depositional zone of the Javaés River, as well as the average annual flow. A) Deforestation area; B) Wetland area; C) Irrigation area and average annual flow from the Barreira da Cruz station. Source: Flow data from the Barreira da Cruz station on the Javaés River (ANA, 2023) and data on deforestation, wetlands, and irrigation from MapBiomas (SOUZA et al., 2020).

4.3 Structural control over lateral migration

The Javaés River, the main affluent of the middle Araguaia, features stretches of simple meandering channel and multichannel stretches with vegetated islands (AQUINO; LATRUBESSE; SOUZA FILHO, 2008; VALENTE; LATRUBESSE; FERREIRA, 2013). Developed in the depositional zone from the reactivation of paleochannels, the Javaés River was influenced by the depositional phases of the Bananal Sedimentary Basin (VALENTE; LATRUBESSE; FERREIRA, 2013). The drainage network is also affected by normal and tailings faults, which result in abrupt curves between rivers that cross the sedimentary basin from S to N (SANTOS; MORAIS, 2017; VALENTE; LATRUBESSE; FERREIRA, 2013). This parallelism is observed in the change in direction of the B, C, F, I stretches (Figure 7), with spatial correspondence in other rivers developed on Bananal Island (SUIZU; LATRUBESSE; BAYER, 2023)

The data from the channel area balance indicated low rates of lateral migration over 37 years, despite the increase in sediment input. The floodplain of the Javaés River is well developed, and it features morphosedimentary records, such as paleochannels and paleolevees, which when combined and connected form a longitudinal axis with high lateral connectivity to the Javaés River (IRON et al., 2016; SANTOS; CHEREM, 2021). Between sections M, secondary channel systems were and I identified connecting the river to the plain, attenuating floods and promoting exchanges between lakes in the Cantão region and the northern tip of Bananal Island (Figures 1, 11A and 12C).

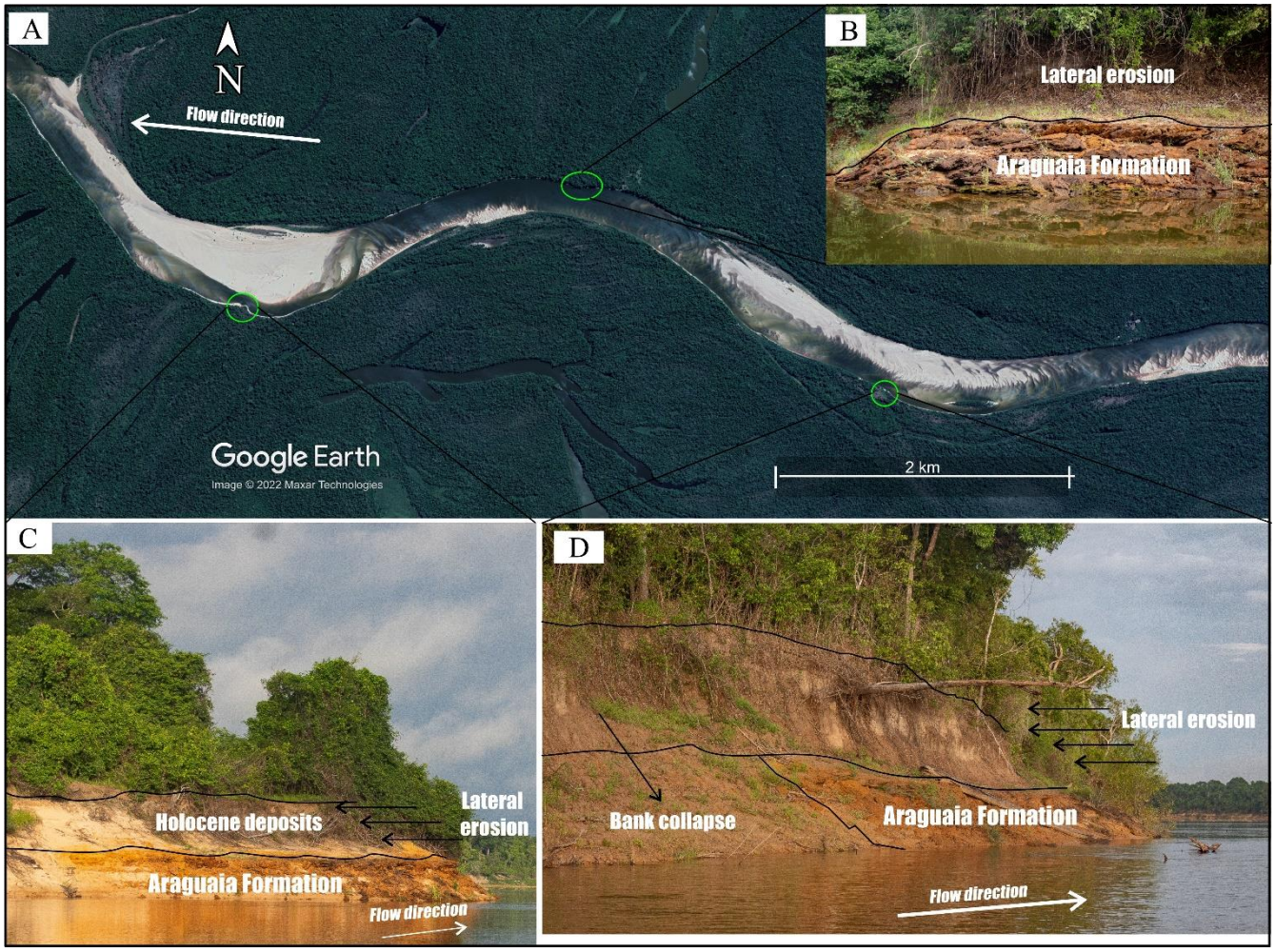

Figure 11. Location of points indicating control of the depositional facies of the Araguaia Formation over the lateral retreat of the banks and orientation of the Javaés River. Source: satellite image from June 7, 2017 (GOOGLE EARTH PRO, 2022) and field images (SANTOS, 2023).

From the analysis conducted by Mendes et al. (2015), which collected sediment and pollen samples from a lake on the Javaés River in section I, it can be seen that over 950 years the deposition rates oscillated between lacustrine and channel regime conditions. Authors such as Suizu, Latrubesse and Bayer (2023) have highlighted the role of the Araguaia/Bananal formation in reducing the lateral migration rates of rivers in the mid-Araguaia region. Analysis of the deposits in the Formoso River, the main tributary of the Javaés, has revealed a confinement and modeling of the channel patterns, imposing less sinuosity (SANTOS, 2016).

Figure 11 shows the semi-confinement of stretches of the Javaés River channels as observed in the field. The gullies show Pleistocene depositional facies, with lateritic sand deposits (Qag1), made up of silty-clayey material with cross-stratification and laterization levels, and sand deposits (Qag2), with a range of shades between yellow, white and grey, associated with fluvial-lacustrine dynamics. The Qag1 facies occurs on the right bank of the Javaés (IBGE, 2007b), bordering parts of the channel between sections A and I, while the Qag2 facies comprises the floodplains of Bananal Island and borders the left bank of the Javaés River between sections A and D. Stretches I,

K and L exhibit a rupture in the control of paleolevees, generating a system of greater sinuosity due to the tailings fault lines (IBGE, 2007b; STROPPER; MARTINS; FRASCA, 2014).

According to Figure 11 and 12B, it can be seen that "points" are residual morphologies associated with the Araguaia formation, which segment the line of the erosion margin and can reduce the efficiency of the channel's flow. During the rainy season, the ravines are eroded by the initial flows that move towards the channel (SANTOS; CHEREM, 2021), creating grooves and gullies (Figure 12A). As the water level rises, the "points" of the Araguaia/Bananal formation are exhumed on the erosion margins, and are exposed on the erosion margins, with the annual removal of the upper strata (Figures 11C and 12B and 12D). Lateral erosion of Holocene deposits destabilizes tree roots, resulting in block fall (Figure 11D and 12D). The lateralized base maintains the dimensions of the smaller bed, giving the ravines a prismatic appearance (MENDES, 2019).

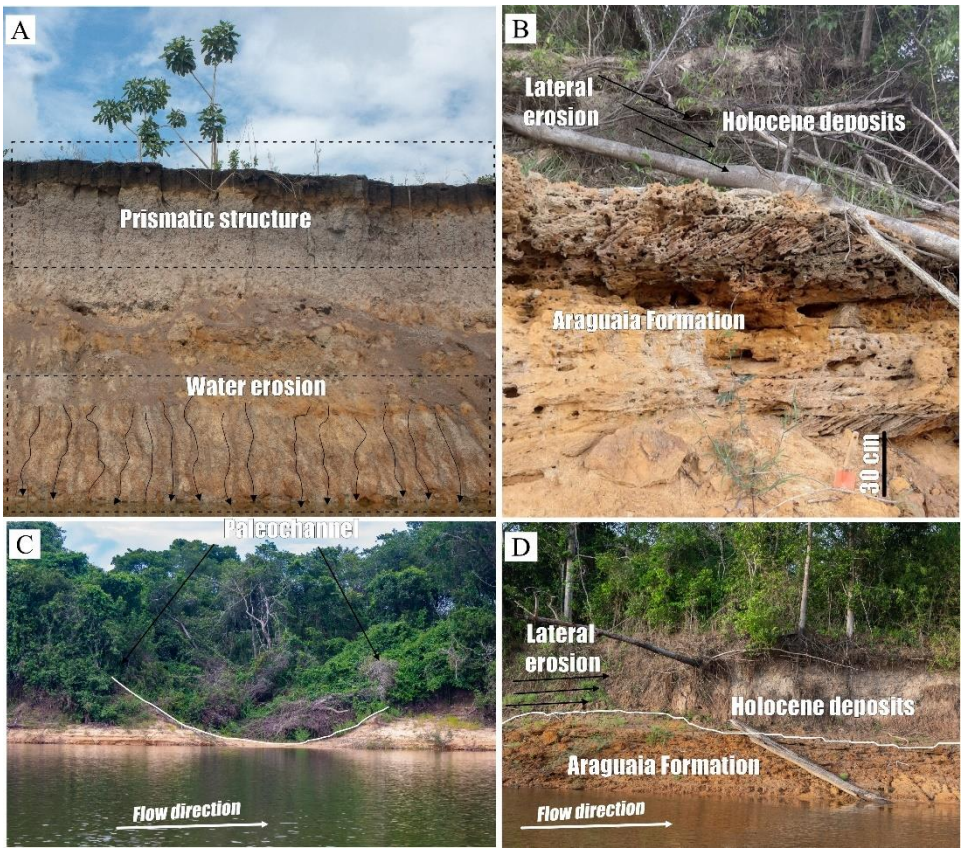

Figure 12. Field records of fluvial processes in the Javaés River. A) Water erosion along the banks of the Javaés River in section K, with prismatic structures and vertical erosion of the bank. B) Outcrop of the Araguaia Formation due to lateral erosion. C) Connection of a paleochannel with the Javaés River. D) Lateral erosion with removal of Holocene deposits and destabilization of trees on the banks. Source: Santos (2023).

Analyzing the results of the Javaés River's features revealed diversified behavior over time. Point bars and lateral bars represent the highest annual percentages of depositional area in the channel (Table 2 and Figure 9). This percentage is inversely related to the trend of the area and frequency of the islands.

The lateral bars are positioned parallel to the channel banks, concentrated in sections A, B, D, F, G, and H (Figure 7). These stretches also display significant spatial differences in the area deposited between 1985 and 2021 (Figures 5, 7 and 8), as well as the lowest sinuosity values (between 1.1 and 1.3). Sinuosity is conlateralred a conditioning characteristic of channel patterns and related depositional features (CHRISTOFOLETTI, 1981; SCHUMM, 1963). A greater sinuosity can reduce the speed of water currents, increase the cross-sectional area and favor deposition and erosion of the banks (SCHUMM, 1985). However, it has also been observed that the permanence of alternating lateral bars can increase the sinuosity of the channel thalweg and modify the bar pattern (STEVAUX, LATRUBESSE, 2017).

On the other hand, the point bars are correlated with more sinuous sections (Figures 7 and 8). It should also be noted that in these sections, structural control can be inferred from the regional arrangement of lineaments

(SANTOS; MORAIS, 2017), which imposes abrupt changes in the direction of sections C, F, I and K (Figure 7). In these sections, the point bars have gentle gradients and can be incorporated more easily into the floodplain, due to a smaller difference between the banks and a greater presence of silt-clay material, generally associated with the meander spines (MONEGAGLIA et al., 2018).

The central bars are more recurrent in the southern segments of the channel, with smaller average and median area dimensions than the other groups, showing high temporal variability in annual frequency. These features are commonly observed in intertwined river systems (SCHUMM, 1963), and can originate from processes that combine phases of erosion and deposition, such as the flow of the bed with the excavation of wells and subsequent deposition losing competence, or bank erosion in lateral bars or point bars during floods, disconnecting the material from the bank (STEVAUX; LATRUBESSE, 2017). The trends of this group in the Javaés River diverge from the behavior observed in the Araguaia River, in mappings also based on images from the LANDSAT series, where linear increases in the frequency of these groups were identified between 2009 and 2018 (SUIZU et al., 2022; 2023).

4.4 Influences on river connectivity and ecogeomorphological dynamics

The increase in the area of sand bars can affect the connectivity of river systems and the ecogeomorphological dynamics of species adapted to hydroclimatic and hydrogemorphological regimes (LENHART; NABER; NIEBER, 2013). When bars increase in size, they can obstruct water flow, reduce the depth of the channel, and hinder the circulation of fish and other aquatic organisms (FERREIRA JÚNIOR; CASTRO, 2003; SIMONCINI et al., 2022). In addition, the increase in bars indicates greater erosion upstream, changes in the dynamics of floods and droughts and impacts on water quality, damaging the health of aquatic ecosystems and the conservation of biodiversity (RESTREPO; KETTNER; SYVITSKI, 2015).

In this sense, the mobility of the sand bars measured in this study could be an important environmental indicator, also considering ecological dynamics. Ecogemorphological studies in the Amazon region and around Bananal Island highlight the importance of these features in turtle reproduction. For example, Tracajás (*Podocnemis unifilis*) inhabit the lower parts of beaches, in regions of small and medium-sized dunes, where the sedimentary texture is coarse due to high flows during rainy periods (ALHO; PÁDUA, 1982; CASTRO; FERREIRA JUNIOR, 2022). The Amazonian turtle (*Podocnemis expansa*), on the other hand, prefers the higher sections of the bars, protected from floods and with fine granulometry.

Ferreira Junior and Castro (2003, 2010) mapped the sand bars between sections I and M and analyzed turtle nesting between 2000 and 2001. The results showed that egg hatching success is linked to sand granulometry, with higher success rates on beaches with fine granulometry. However, nesting and hatching rates were affected differently by river levels in the two years analyzed. In 2000, there was a prolonged drought that was close to the historical average (1977-2000), but there was an intense and rapid rise in the water level for around 30 days. In 2001, the 0 level was reached earlier than predicted in the historical average, and the river level rose early. These studies have also noted that variations in the river flow can affect the humidity and temperature of the sand bars, which can have an impact on the populations of these ectothermic animals. This scenario is even more concerning in the context of climate change, as extreme weather events could become more frequent and affect the survival of these species, in addition to the accentuation of water deficits due to human activities.

5. Conclusions

The study evaluated the two-dimensional morphological settings of a multichannel river in the marginal context of the world's largest river island, Bananal Island. The strategy of composing annual mosaics by the median of the images in the period of least variation in hydrometric elevation was useful for the annual mapping and calculation of the areas of sand bars and water bodies between 1985 and 2021. A significant increase in sediment input by sand bars was observed, which resulted in greater sediment deposition along the river channel.

Analysis of the areas of annual bars by segment throughout the study area has revealed different behaviors. There has been greater deposition and variation in the area of sand bars upstream, in sectors with greater anthropogenic land use, and stability downstream, which correspond to the best preserved areas. On the other hand, while the annual rate of increase in sand bars has increased over the years, the annual rate of mobility of

these bars is decreasing. This suggests that the area balance is consolidating sand bars with a larger area, especially lateral bars, which may result in greater sinuosity in the stretches of the Javaés River analyzed.

A reduction in the bodies of water over the analyzed period, and consequently in the flow of the Javaés River, has been observed. This reduction can be attributed to several factors, including changes in the spatial distribution and volume of regional rainfall in the southwest of the Amazon and in the Cerrado, which result in significant annual reductions in the river's flow. In addition to the intense increase in anthropogenic activities in the region during the same period analyzed. This is accentuated by the intense use of irrigation. The transfer of water to agricultural areas modified by intensive irrigation contributes to the water deficit in the region, triggering a negative cascade effect that results in increased sedimentation in the river and degradation of aquatic ecosystems. Therefore, changes in precipitation patterns, along with the expansion of the occupation of wetlands converted into pastures and irrigation areas, are the main environmental factors affecting the mid-Araguaia region and have a direct impact on the dynamics of the Javaés River, affecting its morphosedimentary balance and fluvial connectivity.

Author's contributions: Conception, D.A.R.S.; methodology, D.A.R.S. and É.H.C.; software, D.A.R.S. and É.H.C.; validation, D.A.R.S. and É.H.C.; formal analysis, D.A.R.S., É.H.C. and L.F.S.C.; research, D.A.R.S., É.H.C. and L.F.S.C.; resources, É.H.C. and L.F.S.C.; data preparation, D.A.R.S.; article writing, D.A.R.S., É.H.C. and L.F.S.C.; revision, É.H.C. and L.F.S.C.; supervision, É.H.C. and L.F.S.C. All authors have read and agreed with the published version of the manuscript.

Funding: É.H.C. is research fellow of Brazilian National Council for Scientific and Technological Development - CNPq/Brazil (#310198/2022-4).

Acknowledgments: The authors thank the "Coordenação de Aperfeiçoamento de Pessoal de Nível Superior – Brasil" (CAPES) for the doctoral scholarship awarded to the first author.

Conflict of Interest: The authors declare not having any conflict of interest.

References

1. AGNIHOTRI, A. K.; OHRI, A.; MISHRA, S. Channel planform dynamics of lower Ramganga River, Ganga basin, GIS and remote sensing analyses. **Geocarto International**, v. 35, n. 9, p. 934–953, 2020. DOI: 10.1080/10106049.2018.1552323
2. AGUDELO, J.; ARIAS, P.A.; VIEIRA, S.C.; MARTÍNEZ, A. Influence of longer dry seasons in the Southern Amazon on patterns of water vapor transport over northern South America and the Caribbean. **Climate Dynamics**, v. 52, n. 5, p. 2647–2665, 2019. DOI: 10.1007/s00382-018-4285-1
3. ALHO, C. J. R.; PÁDUA, L. F. M. Sincronia entre o regime de vazante do rio e o comportamento de nidificação da tartaruga da Amazônia Podocnemis expansa (Testudinata: Pelomedusidae). **Acta Amazonica**, v. 12, n. 2, p. 323–326, 1982. DOI: 10.1590/1809-43921982122323
4. ALVES, V. E. L. Expansão do Agronegócio e os Impactos Socioambientais na Região de Cerrados do Centro-Norte do Brasil (MATOPIBA). **Confins**, n. 45, 2020. DOI: 10.4000/confins.28049
5. ANACHE, J. A. A.; WENDLAND, E.; ROSALEM, L. M. P.; YOULTON, C.; OLIVEIRA, P. T. S. Hydrological trade-offs due to different land covers and land uses in the Brazilian Cerrado. **Hydrology and Earth System Sciences**, v. 23, n. 3, p. 1263–1279, 2019. DOI: 10.5194/hess-23-1263-2019
6. AQUINO, S.; LATRUBESSE, E. M.; SOUZA FILHO, E. E. Relações entre o regime hidrológico e os ecossistemas aquáticos da planície aluvial do rio Araguaia. **Acta Scientiarum. Biological Sciences**, v. 30, n. 4, p. 361–369, 2008. DOI: 10.4025/actascibiolsci.v30i4.5866
7. ARVOR, D.; FUNATSU, B.M.; MICHOT, V.; DUBREUIL, V. Monitoring Rainfall Patterns in the Southern Amazon with PERSIANN-CDR Data: Long-Term Characteristics and Trends. **Remote Sensing**, v. 9, n. 9, p. 889, 2017. DOI: 10.3390/rs9090889
8. BARROS, L. F. DE P.; MAGALHÃES JÚNIOR, A. P.; COTA, G. E. M. Morfogênese fluvial. Em: **Hidrogeomorfologia: Formas, processos e registros sedimentares fluviais.** Rio de Janeiro: Antônio Pereira Magalhães Júnior; Luiz Fernando de Paula Barros, v. 1p. 121–161, 2020.
9. BAYER, M. **Diagnóstico dos processos de erosão/assoreamento na planície aluvial do rio Araguaia: entre Barra do Garças e Cocalinho**. 2002. p.138.Dissertação (Mestrado em Geografia) – Instituto de Estudos Sócio-Ambientais, Universidade Federal de Goiás, Goiânia.2002.
10. BAYER, M.; ASSIS, P.C.; SUIZU, T. M.; GOMES, M. C. Mudança no uso e cobertura da terra na bacia hidrográfica do rio Araguaia e seus reflexos nos recursos hídricos, o trecho médio do rio Araguaia em Goiás. **Confins**, n. 48, 2020. DOI: 10.4000/confins.33972

11. BETTIOL, G. M. **Conformidade entre dados biofísicos orbitais e terrestres para o zoneamento agroclimático, identificação espaço-temporal de tendências de precipitação e suas relações com uso e cobertura da terra no bioma cerrado**. 2021. 199 f. Dissertação (Mestrado em Ciências Ambientais) - Universidade Federal de Goiás, Goiânia, 2021.
12. BLANCO, L. S.; PORTELLA, D. A. P. DA C.; SANTOS, J. L. A.; BARBOSA, S. C. O.; DIAS, J. L. R. O projeto de modernização brasileira e suas consequências socioambientais no Matopiba. **Boletim Paulista de Geografia**, v. 1, n. 107, p. 121–136, 2022.
13. BOOTHROYD, R. J.; WILLIAMS, R. D.; HOEY, T. B.; BARRETT, B.; PRASOJO, O. A. Applications of Google Earth Engine in fluvial geomorphology for detecting river channel change. **Wiley Interdisciplinary Reviews: Water**, v. 8, n. 1, p. e21496, 2021. DOI: 10.1002/wat2.1496
14. BORMA, L. S. et al. Atmosphere and hydrological controls of the evapotranspiration over a floodplain forest in the Bananal Island region, Amazonia. **Journal of Geophysical Research: Biogeosciences**, v. 114, n. G1, p. 1003, 2009. DOI: 10.1029/2007JG000641
15. BORRA, S.; THANKI, R.; DEY, N. **Satellite Image Analysis: Clustering and Classification**. Singapore: Springer Singapore, 2019.
16. BREIMAN, L. Random forests. **Machine Learning**, v. 45, n. 1, p. 5–32, 2001. DOI: 10.1023/A:1010933404324
17. BRIERLEY, G.; FRYIRS, K. A. **Geomorphology and River Management. Applications of the River Styles Framework**. 1. ed. Oxford: Blackwell Science, 2005.
18. CAMPOS, J. O.; CHAVES, H. M. L. Tendências e Variabilidades nas Séries Históricas de Precipitação Mensal e Anual no Bioma Cerrado no Período 1977-2010. **Revista Brasileira de Meteorologia**, v. 35, n. 1, p. 157–169, 2020. DOI: 10.1590/0102-7786351019
19. CARLING, P. A. et al. Are equilibrium multichannel networks predictable? The case of the regulated Indus River, Pakistan. **Geomorphology**, v. 302, p. 20–34, 2018. DOI: 10.1016/j.geomorph.2017.09.021
20. CASTRO, P. de T. A.; FERREIRA JÚNIOR, P. D. Caracterização ecogeomorfológica das áreas de desova de quelônios de água doce (gênero podocnemis) no entorno da Ilha do Bananal, Rio Araguaia. **Revista Geografias**, v. 4, n. 2, p. 15–22, 2022. DOI: 10.35699/2237-549X.13247.
21. CASTRO, S. S. Erosão hídrica na alta bacia do rio Araguaia: distribuição, condicionantes, origem e dinâmica atual. **Revista do Departamento de Geografia**, v. 17, p. 38–60, 2005. DOI: 10.7154/RDG.2005.0017.0004
22. CASTRO, W. S.; CAMPOS, A. B.; ZANCOPÉ, M. H. C. A influência dos materiais das margens e da vegetação ciliar na erosão de meandros: o caso do rio Claro, afluente do rio Araguaia. **Revista Brasileira de Geomorfologia**, v. 20, n. 3, p. 623–640, 2019. DOI: 10.20502/rbg.v20i3.1584
23. CHARLTON, R. **Fundamentals of fluvial geomorphology**. 1. ed. London: Routledge, 2008.
24. CHEN, C.-N.; TFWALA, S. S.; TSAI, C.-H. Climate Change Impacts on Soil Erosion and Sediment Yield in a Watershed. **Water**, v. 12, n. 8, p. 2247, 2020. DOI: 10.3390/w12082247
25. CHRISTOFOLETTI, A. **Geomorfologia fluvial**. São Paulo: E. Blücher, 1981. v. 1
26. COE, M. T.; BRANDO, P.M.; DEEGAN, L.A.; MACEDO, M.N.; NEILL, C.; SILVÉRIO, D.V. The Forests of the Amazon and Cerrado Moderate Regional Climate and Are the Key to the Future. **Tropical Conservation Science**, v. 10, 2017. DOI: 10.1177/1940082917720671
27. COE, M. T.; LATRUBESSE, E.M., FERREIRA, M.E.; AMSLER, M. L. The effects of deforestation and climate variability on the streamflow of the Araguaia River, Brazil. **Biogeochemistry**, v. 105, n. 1, p. 119–131, 2011. DOI: 10.1007/s10533-011-9582-2
28. DE HIPT, F. O. et al. Modeling the impact of climate change on water resources and soil erosion in a tropical catchment in Burkina Faso, West Africa. **Catena**, v. 163, p. 63–77, 2018. DOI: 10.1016/j.catena.2017.11.023
29. DIAS, C. M. et al. Modelling and numerical simulation of the velocity field in the Parque Estadual do Cantão (TO), Brazil. **Mathematical and Computer Modelling**, v. 53, n. 7–8, p. 1575–1581, 2011. DOI: 10.1016/j.mcm.2010.06.021
30. DIODATO, N. et al. The Rise of Climate-Driven Sediment Discharge in the Amazonian River Basin. **Atmosphere**, v. 11, n. 2, p. 208, 2020. DOI: 10.3390/atmos11020208
31. DURIGAN, G. et al. Cerrado wetlands: multiple ecosystems deserving legal protection as a unique and irreplaceable treasure. **Perspectives in Ecology and Conservation**, v. 20, n. 3, p. 185–196, 2022. DOI: 10.1016/j.pecon.2022.06.002
32. FAGUNDES, F. **Análise do uso da água para irrigação na bacia hidrográfica do Rio Formoso**. 2021. 83f. Dissertação (Mestrado Profissional em Engenharia Ambiental) – Universidade Federal do Tocantins, Programa de Pós-Graduação em Engenharia Ambiental, Palmas, 2021.
33. FERREIRA JÚNIOR, P. D.; CASTRO, P. DE T. A. Geological control of Podocnemis expansa and Podocnemis unifilis nesting areas in Rio Javaés, Bananal Island, Brazil. **Acta Amazonica**, v. 33, n. 3, p. 445–468, 2003. DOI: 10.1590/S0044-59672003000300010

34. FERREIRA JÚNIOR, P. D.; CASTRO, P. DE T. A. Nesting ecology of Podocnemis expansa (Schweigger, 1812) and Podocnemis unifilis (Troschel, 1848) (Testudines, Podocnemididae) in the Javaés River, Brazil. **Brazilian Journal of Biology**, v. 70, p. 85–94, 2010. DOI: 10.1590/S1519-69842010000100012
35. FERREIRA, M. E.; FERREIRA, L. G.; LATRUBESSE, E. M.; MIZIARA, F. High resolution remote sensing based quantification of the remnant vegetation cover in the Araguaia river basin, central Brazil. **International Geoscience and Remote Sensing Symposium (IGARSS)**, v. 4, n. 1, 2008. DOI: 10.1109/IGARSS.2008.4779828
36. FERREIRA, M. E.; FERREIRA, L. G.; LATRUBESSE, E. M.; MIZIARA, F. Considerations about the land use and conversion trends in the savanna environments of Central Brazil under a geomorphological perspective. **Journal of Land Use Science**, v. 11, n. 1, p. 33–47, 2016. DOI: 10.1080/1747423X.2013.845613
37. FIENER, P.; NEUHAUS, P.; BOTSCHEK, J. Long-term trends in rainfall erosivity–analysis of high resolution precipitation time series (1937–2007) from Western Germany. **Agricultural and Forest Meteorology**, v. 171–172, p. 115–123, 2013. DOI: 10.1016/j.agrformet.2012.11.011
38. FLEISCHMANN, A. S. et al. Avaliação da seca de 2016 do Rio Javaés (bacia do Rio Araguaia) com uso de dados de múltiplos satélites. **Anais do XVII Simpósio Brasileiro de Sensoriamento Remoto**, p. 5033–5040, 2017.
39. FRAGAL, E.H.; CREMON, É. H. Catalogação de imagens orbitais a partir da cobertura de nuvem e nível fluviométrico do Alto rio Paraná. **Boletim de Geografia**, v. 30, n. 3, p. 173-179, 2012. DOI: https://doi.org/10.4025/bolgeogr.v30i3.17415
40. FRYIRS, K. A.; BRIERLEY, G. J. **Geomorphic Analysis of River Systems**. Chichester, UK: Wiley-Blackwell, 2012.
41. FUNATSU, B. M. et al. Assessing precipitation extremes (1981–2018) and deep convective activity (2002–2018) in the Amazon region with CHIRPS and AMSU data. **Climate Dynamics**, v. 57, n. 3, p. 827–849, 2021. DOI: 10.1007/s00382-021-05742-8
42. GILVEAR, D. J.; WINTERBOTTOM, S. J. Channel change and flood events since 1783 on the regulated river tay, Scotland: Implications for flood hazard management. **Regulated Rivers: Research & Management**, v. 7, n. 3, p. 247–260, 1992. DOI: 10.1002/rrr.3450070304
43. GOMES, D. J. C. et al. Flow variability in the Araguaia River Hydrographic Basin influenced by precipitation in extreme years and deforestation. **Revista Brasileira de Ciências Ambientais**, v. 57, n. 3, p. 451–466, 2022. DOI: 10.5327/Z2176-94781358
44. GOMES, D. J. C. et al. Vulnerabilidade à erosão hídrica do solo, bacia hidrográfica do rio Araguaia. **Revista Brasileira de Geografia Física**, v. 14, n. 2, p. 816–833, 2021. DOI: 10.26848/rbgf.v14.2.p816-833.
45. GOMES, D. J. C.; FERREIRA, N. S.; LIMA, A. M. M. Tendências de variabilidade espaço-temporal pluviométrica na bacia hidrográfica do rio Araguaia. **Enciclopédia Biosfera**, v. 16, n. 29, p. 1421–1433, 30 jun. 2019. DOI: 10.18677/EnciBio_2019A126
46. GOOGLE EARTH PRO. Imagem de satélite do rio Javaés. Captura de tela do Google Earth Pro]. Earth, versão 7.3.6. Disponível em: https://earth.google.com/web/@-9.9787813,-50.04801066,177.2026793a,2966.85861877d,35y,359.04479747h,0t,0r/data=OgMKATA Acesso em: 12/12/2022
47. GORELICK, N. et al. Google Earth Engine: Planetary-scale geospatial analysis for everyone. **Remote Sensing of Environment**, v. 202, p. 18–27, 1 dez. 2017. DOI: 10.1016/j.rse.2017.06.031
48. GRILL, G.; LEHNER, B.; THIEME, M. et al. Mapping the world's free-flowing rivers. **Nature**, v. 569, n. 7755, p. 215–221, 2019. DOI: 10.1038/s41586-019-1111-9
49. GUIMARÃES, U. S.; NARVAES, I. D. S.; GALO, M. DE L. B. T. Aplicação de dados ERS, Envisat e Sentinel para detecção de mudanças nos ambientes costeiros amazônicos. **Revista Brasileira de Geomorfologia**, v. 18, n. 2, p. 257–278, 2017. DOI: 10.20502/rbg.v18i2.998
50. GURNELL, A. M.; DOWNWARD, S. R.; JONES, R. Channel planform change on the river dee meanders, 1876–1992. **Regulated Rivers: Research & Management**, v. 9, n. 4, p. 187–204, 1994. DOI: 10.1002/rrr.3450090402
51. HAGHTALAB, N.; MOORE, N., HEERSPINK, B.P. et al. Evaluating spatial patterns in precipitation trends across the Amazon basin driven by land cover and global scale forcings. **Theoretical and Applied Climatology**, v. 140, n. 1–2, p. 411–427, 2020. DOI: 10.1007/s00704-019-03085-3
52. HOFMANN, G. S. et al. Changes in atmospheric circulation and evapotranspiration are reducing rainfall in the Brazilian Cerrado. **Scientific Reports**, v. 13, n. 1, p. 11236, 2023. DOI: 10.1038/s41598-023-38174-x
53. HOOKE, J. M. An analysis of the processes of river bank erosion. **Journal of Hydrology**, v. 42, n. 1–2, p. 39–62, 1 jun. 1979. DOI: 10.1016/0022-1694(79)90005-2
54. HOOKE, J. M. Magnitude and distribution of rates of river bank erosion. **Earth Surface Processes**, v. 5, n. 2, p. 143–157, 1980. DOI: 10.1002/esp.3760050205
55. HUNKE, P. et al. The Brazilian Cerrado: assessment of water and soil degradation in catchments under intensive agricultural use. **Ecohydrology**, v. 8, n. 6, p. 1154–1180, 2015. DOI: 10.1002/eco.1573

56. IBGE. **Estado do Tocantins: Geologia**. Rio de Janeiro, IBGE: Coordenação de Recursos Naturais e Estudos Ambientais, 2007b.
57. IBGE. **Estado do Tocantins: Geomorfologia**. Rio de Janeiro,IBGE - Coordenação de Recursos Naturais e Estudos Ambientais, 2007a.
58. IELPI, A. et al. The impact of vegetation on meandering rivers. **Nature Reviews Earth & Environment**, v. 3, n. 3, p. 165–178, 2022. DOI: 10.1038/s43017-021-00249-6
59. IRION, G.; NUNES, G.M.; NUNES-DA-CUNHA, C. et al. Araguaia river floodplain: size, age, and mineral composition of a large tropical savanna wetland. **Wetlands**, v. 36, p. 945–956, 2016. DOI: 10.1007/s13157-016-0807-y
60. ISIKDOGAN, F.; BOVIK, A.; PASSALACQUA, P. RivaMap: An automated river analysis and mapping engine. **Remote Sensing of Environment**, v. 202, p. 88–97, 2017. DOI: 10.1016/j.rse.2017.03.044
61. LANGHORST, T.; PAVELSKY, T. Global Observations of Riverbank Erosion and Accretion From Landsat Imagery. **Journal of Geophysical Research: Earth Surface**, v. 128, n. 2, e2022JF006774, 2023. DOI: 10.1029/2022JF006774
62. LATRUBESSE, E. M. et al. Fostering water resource governance and conservation in the Brazilian Cerrado biome. **Conservation Science and Practice**, v. 1, n. 9, p. e77, 2019. DOI: 10.1111/csp2.77
63. LATRUBESSE, E. M. et al. The geomorphologic response of a large pristine alluvial river to tremendous deforestation in the South American tropics: The case of the Araguaia River. **Geomorphology**, v. 113, n. 3–4, p. 239–252, 2009. DOI: 10.1016/j.geomorph.2009.03.014
64. LATRUBESSE, E. M. Patterns of anabranching channels: The ultimate end-member adjustment of mega rivers. **Geomorphology**, v. 101, n. 1–2, p. 130–145, 2008. DOI: 10.1016/j.geomorph.2008.05.035
65. LATRUBESSE, E. M.; STEVAUX, J. C. Geomorphology and environmental aspects of the Araguaia Fluvial Basin, Brazil. **Zeitschrift für Geomorphologie**, Supplement Issues, p. 109–127, 2002.
66. LATRUBESSE, E. M.; STEVAUX, J. C.; SINHA, R. Tropical rivers. **Geomorphology**, v. 70, n. 3–4, p. 187–206, 2005. DOI: 10.1016/j.geomorph.2005.02.005
67. LAWLER, D. M. The measurement of river bank erosion and lateral channel change: A review. **Earth Surface Processes and Landforms**, v. 18, n. 9, p. 777–821, 1993. DOI: 10.1002/esp.3290180905
68. LENHART, C.; NABER, J.; NIEBER, J. Impacts of Hydrologic Change on Sandbar Nesting Availability for Riverine Turtles in Eastern Minnesota, USA. **Water**, v. 5, n. 3, p. 1243–1261, 2013. DOI: 10.3390/w5031243
69. LI, H. et al. A Google Earth Engine-enabled software for efficiently generating high-quality user-ready Landsat mosaic images. **Environmental modelling & software**, v. 112, p. 16-22, 2019. DOI: 10.1016/j.envsoft.2018.11.004
70. MACHADO, C. A.; DOS SANTOS, D. A. R. Influências do controle estrutural na formação de ilhas e planícies de inundação na represa da Usina Hidrelétrica do Estreito no rio Tocantins, Filadélfia (TO). **Sociedade e Território**, v. 32, n. 2, p. 26–46, 2020. DOI: 10.21680/2177-8396.2020v32n2ID20484
71. MAGALHÃES JÚNIOR, A. P.; BARROS, L. F. DE P. Depósitos fluviais e feições deposicionais. In: **Hidrogeomorfologia: Formas, processos e registros sedimentares fluviais.** Rio de Janeiro: Antônio Pereira Magalhães Júnior; Luiz Fernando de Paula Barros, 2020. v. 1p. 259–278.
72. MANCHOLA, O. E. P.; MORAIS, F. DE. Caracterização morfométrica de feições doliniformes na Planície do Araguaia. **Sociedade & Natureza**, v. 35, n. 1, 2023. DOI: 10.14393/SN-v35-2023-67351
73. MARCUZZO, F. F. ORONHA; ROMERO, V. Influência do El Niño e La Niña na precipitação máxima diária do estado de Goiás. **Revista Brasileira de Meteorologia**, v. 28, p. 429–440, 2013. DOI: 10.1590/S0102-77862013000400009
74. MARENGO, J. A.; JIMENEZ, J. C.; ESPINOZA, J. C. et al. Increased climate pressure on the agricultural frontier in the Eastern Amazonia–Cerrado transition zone. **Scientific Reports**, v. 12, n. 1, p. 457, 2022. DOI: 10.1038/s41598-021-04241-4
75. MARTINS, A. K. E. et al. Relações solo-geoambiente em áreas de ocorrências de Ipucas na planície do Médio Araguaia - Estado de Tocantins. **Revista Árvore**, v. 30, n. 2, p. 297–310, abr. 2006. DOI: 10.1590/S0100-67622006000200017
76. MARTINS, P. R. et al. Terrain units, land use and land cover, and gross primary productivity of the largest fluvial basin in the Brazilian Amazonia/Cerrado ecotone: The Araguaia River basin. **Applied Geography**, v. 127, p. 102379, 2021. DOI: 10.1016/j.apgeog.2020.102379
77. MCLEOD, A. I.; MAINTAINER, A. I. **Package 'Kendall'**. R Software. London, UK, 2015.
78. MENDES, L. A. DA S. et al. Vegetational changes during the last millennium inferred from a palynological record from the Bananal Island, Tocantins, Brazil. **Acta Amazonica**, v. 45, n. 2, p. 215–230, 2015. DOI: 10.1590/1809-4392201402265
79. MENDES, L. A. S. **Dinâmica da paisagem na porção norte da Ilha do Bananal-TO e adjacências ao longo do Quaternário tardio.** 2019. 130 f. tese (Doutorado em Geologia e Geoquímica) – Instituto de Geociências, Universidade Federal do Pará, Belém, 2019.

80. MONEGAGLIA, F. et al. Automated extraction of meandering river morphodynamics from multitemporal remotely sensed data. **Environmental Modelling & Software**, v. 105, p. 171–186, 2018. DOI: 10.1016/j.envsoft.2018.03.028
81. MORAIS, R. P. **A planície aluvial do médio rio Araguaia: processos geomorfológicos e suas implicações ambientais**. 2006. 178 f. Tese (Doutorado em Ciências Ambientais) - Universidade Federal de Goiás, Goiânia, 2006.MORAIS, P. B.; JÚNIOR, S. N.; MENEZES MARTINS, I. C. Análise de sustentabilidade do projeto hidroagrícola Javaés/Lagoa, no Estado do Tocantins. **Cadernos de Ciência & Tecnologia**, v. 34, n. 1, p. 83–111, 2017. DOI: 10.35977/0104-1096.cct2017.v34.26297
82. MU, Y.; JONES, C. An observational analysis of precipitation and deforestation age in the Brazilian Legal Amazon. **Atmospheric Research**, v. 271, p. 106122, 2022. DOI: 10.1016/j.atmosres.2022.106122
83. NASCIMENTO, D. T. F.; NOVAIS, G. T. Clima do Cerrado: dinâmica atmosférica e características, variabilidades e tipologias climáticas. **Eliséé**, v. 9, n. 2, p. e922021, 2020.
84. NGUYEN, Q. H. et al. Influence of data splitting on performance of machine learning models in prediction of shear strength of soil. **Mathematical Problems in Engineering**, v. 2021, n. Special Issue, p. 1–15, 2021. DOI: 10.1155/2021/4832864
85. NYBERG, B. et al. Geometric attribute and shape characterization of modern depositional elements: A quantitative GIS method for empirical analysis. **Computers & Geosciences**, v. 82, p. 191–204, 2015. DOI: 10.1016/j.cageo.2015.06.003
86. PEIXOTO, J. M. A.; NELSON, B. W.; WITTMANN, F. Spatial and temporal dynamics of river channel migration and vegetation in central Amazonian white-water floodplains by remote-sensing techniques. **Remote Sensing of Environment**, v. 113, n. 10, p. 2258–2266, 2009. DOI: 10.1016/j.rse.2009.06.015
87. PELICICE, F. M. et al. Large-scale Degradation of the Tocantins-Araguaia River Basin. **Environmental Management**, v. 68, n. 4, p. 445–452, 2021. DOI: 10.1007/s00267-021-01513-7
88. PINTO, C. T.; JING, X.; LEIGH, L. Evaluation Analysis of Landsat Level-1 and Level-2 Data Products Using In Situ Measurements. **Remote Sensing**, vol. 12, n. 16, 2597, 2020. DOI: 10.3390/rs12162597
89. QGIS Development Team. **QGIS Geographic Information System (versão 3.18)**. 2022. Disponível em: <https://qgis.org/pt_BR/site/>.
90. R Core Team. **R: A Language and Environment for Statistical Computing**. Vienna, Áustria, 2020. Disponível em: <https://www.r-project.org/>.
91. RADAMBRASIL, M. DAS M. E ENERGIA. S. G. **Folha SC. 22. Tocantins: Geologia, geomorfologia, pedologia, vegetação e uso potencial da terra**. Rio de Janeiro: Ministério das Minas e Energia, Secretaria Geral, 1981.
92. RESTREPO, J. D.; KETTNER, A. J.; SYVITSKI, J. P. M. Recent deforestation causes rapid increase in river sediment load in the Colombian Andes. **Anthropocene**, v. 10, p. 13–28, 2015. DOI: 10.1016/j.ancene.2015.09.001
93. ROY, S. Role of transportation infrastructures on the alteration of hillslope and fluvial geomorphology. **The Anthropocene Review**, v. 9, n. 3, p. 344–378, 2022. DOI: 10.1177/2053019622112837
94. ROZO, M. G.; NOGUEIRA, A. C.; CASTRO, C. S. Remote sensing-based analysis of the planform changes in the upper Amazon River over the period 1986–2006. **Journal of South American Earth Sciences**, v. 51, p. 28–44, 2014. DOI: 10.1016/j.jsames.2013.12.004
95. SANG, Y. F.; WANG, Z.; LIU, C. Comparison of the MK test and EMD method for trend identification in hydrological time series. **Journal of Hydrology**, v. 510, p. 293–298, 2014. DOI: 10.1016/j.jhydrol.2013.12.039
96. SANTANA, N. M. P. et al. Chuvas, erosividade, erodibilidade, uso do solo e suas relações com focos erosivos lineares na alta bacia do rio Araguaia. **Sociedade & Natureza**, v. 19, p. 103–121, 2007. DOI: 10.1590/S1982-45132007000200007
97. SANTOS, D. A. R. **A rede de drenagem e seu significado geomorfológico: anomalias de drenagens e tectônica recente na bacia do rio Formoso, Tocantins**. Mestrado em Geografia—Porto Nacional: Universidade Federal do Tocantins, 2016.
98. SANTOS, D. A. R. **Javaés Expedition: Field Photographs of a Brazilian River**, 2023. DOI: 10.5281/zenodo.7994827
99. SANTOS, D. A. R. S.; CHEREM, L. F. S. Análise de dados de Sensoriamento Remoto nas estimativas de variabilidade espacial e temporal de superfícies de inundação na planície fluvial do rio Javaés, TO. **Caderno de Geografia**, v. 31, n. 67, p. 1169–1169, 2021. DOI: 10.5752/P.2318-2962.2021v31n67p1169
100. SANTOS, D. A. R.; MORAIS, F. A assimetria de bacias hidrográficas e influências litoestruturais na geomorfologia do rio Formoso, TO. **Caminhos de Geografia**, v. 18, n. 61, p. 180–199, 2017. DOI: 10.14393/RCG186112
101. SANTOS, E. B.; LUCIO, P. S.; SILVA, C. M. S. Precipitation regionalization of the Brazilian Amazon. **Atmospheric Science Letters**, v. 16, n. 3, p. 185–192, 2015. DOI: https://doi.org/10.1002/asl2.535
102. SCHUMM, S. A. Patterns of alluvial rivers. **Annual Review of Earth and Planetary Sciences**, v. 13, n. 1, p. 5–27, 1985. DOI: 10.1146/annurev.ea.13.050185.000253
103. SCHUMM, S. A. Sinuosity of alluvial rivers on the Great Plains. **Geological Society of America Bulletin**, v. 74, n. 9, p. 1089–1100, 1963. DOI: 10.1130/0016-7606(1963)74[1089:SOAROT]2.0.CO;2

104. SEAR, D.; NEWSON, M. Fluvial geomorphology: its basis and methods. In: SEAR, D. A.; NEWSON, M. D.; THORNE, C. R. (Eds.). **Guidebook of applied fluvial geomorphology**. London: Thomas Telford Ltd, 2010. p. 1–31.
105. SEN, P. K. Estimates of the regression coefficient based on Kendall's tau. **Journal of the American statistical association**, v. 63, n. 324, p. 1379–1389, 1968. DOI: 10.2307/2285891
106. SHIMABUKURO, Y. E.; DUTRA, A. C.; ARAI, E. Modelo Linear de Mistura Espectral: Conceitos Teóricos, Algoritmos e Aplicações em Estudos na Amazônia Legal. **Revista Brasileira de Cartografia**, v. 72, p. 1140–1169, 30 dez. 2020. DOI: 10.14393/rbcv72nespecial50anos-56559
107. SHIMABUKURO, Y. E.; SMITH, J. A. The Least-Squares Mixing Models to Generate Fraction Images Derived From Remote Sensing Multispectral Data. **IEEE Transactions on Geoscience and Remote Sensing**, v. 29, n. 1, p. 16–20, 1991. DOI: 10.1109/36.103288
108. SILVA, A.; SOUZA FILHO, E. E.; NEVES, S. M. A. S. Erosão marginal e sedimentação no rio Paraguai no município de Cáceres (MT). **Brazilian Journal of Geology**, v. 41, n. 1, p. 76–84, 2011. DOI: 10.25249/0375-7536.20114117684
109. SILVA, L. L. O papel do estado no processo de ocupação das áreas de cerrado entre as décadas de 60 e 80. **Caminhos de Geografia**, v. 1, n. 2, p. 24–36, 2000. DOI: 10.14393/RCG2215251
110. SIMONCINI, M. S. et al. Hydrological Effects on the Reproduction of the Giant South American River Turtle Podocnemis expansa (Testudines: Podocnemididae). **Ichthyology & Herpetology**, v. 110, n. 3, p. 547–560, 2022. DOI: 10.1643/h2020152
111. SOUZA, C. M. et al. Reconstructing Three Decades of Land Use and Land Cover Changes in Brazilian Biomes with Landsat Archive and Earth Engine. **Remote Sensing**, v. 12, n. 17, p. 2735, 2020. DOI: 10.3390/rs12172735
112. STEVAUX, J. C.; LATRUBESSE, E. M. **Geomorfologia fluvial**. São Paulo: Oficina de Textos, 2017.
113. STROPPER, J. L.; MARTINS, E. G.; FRASCA, A. A. S. **Carta geológica: folha Santa Teresinha, SC. 22-ZA**. CPRM, , 2014.
114. SUIZU, T. M. et al. Resposta da morfologia do médio-curso superior do Rio Araguaia às mudanças no regime hidrossedimentar no período 2001-2018. **Revista Brasileira de Geomorfologia**, v. 23, n. 2, p. 1420–1434, 2022. DOI: 10.20502/rbg.v23i2.2088
115. SUIZU, T. M.; LATRUBESSE, E. M.; BAYER, M. Geomorphic diversity of the middle Araguaia River, Brazil: A segment-scale classification to support river management. **Journal of South American Earth Sciences**, v. 121, p. 104166, 2023. DOI: 10.1016/j.jsames.2022.104166
116. TOBÓN-MARÍN, A.; CAÑÓN BARRIGA, J. Analysis of changes in rivers planforms using Google Earth Engine. **International Journal of Remote Sensing**, v. 41, n. 22, p. 8654–8681, 2020. DOI: 10.1080/01431161.2020.1792575
117. VALENTE, C. R.; LATRUBESSE, E. M. Fluvial archive of peculiar avulsive fluvial patterns in the largest Quaternary intracratonic basin of tropical South America: the Bananal Basin, Central-Brazil. **Palaeogeography, Palaeoclimatology, Palaeoecology**, v. 356, p. 62–74, 2012. DOI: 10.1016/j.palaeo.2011.10.002
118. VALENTE, C. R.; LATRUBESSE, E. M.; FERREIRA, L. G. Relationships among vegetation, geomorphology and hydrology in the Bananal Island tropical wetlands, Araguaia River basin, Central Brazil. **Journal of South American Earth Sciences**, v. 46, p. 150–160, 2013. DOI: 10.1016/j.jsames.2012.12.003
119. VERCRUYSSE, K.; GRABOWSKI, R. C. Human impact on river planform within the context of multi-timescale river channel dynamics in a Himalayan river system. **Geomorphology**, v. 381, p. 107659, 2021. DOI: 10.1016/j.geomorph.2021.107659
120. VOLKEN, N. J. et al. Analyzing the impact of agricultural water-demand management on water availability in the Urubu River basin – Tocantins, Brazil. **Ambiente e Agua - An Interdisciplinary Journal of Applied Science**, v. 17, n. 4, p. 1–23, 2022. DOI: 10.4136/ambi-agua.2847
121. WANG, C. et al. Channel bar feature extraction for a mining-contaminated river using high-spatial multispectral remote-sensing imagery. **GIScience & Remote Sensing**, v. 53, n. 3, p. 283–302, 2016. DOI: 10.1080/15481603.2016.1148229
122. WULDER, M. A. et al. Fifty years of Landsat science and impacts. **Remote Sensing of Environment**, v. 280, p. 113195, 2022. DOI: 10.1016/j.rse.2022.113195
123. ZALLES, V. et al. Rapid expansion of human impact on natural land in South America since 1985. **Science Advances**, v. 7, n. 14, 2021. DOI: 10.1126/sciadv.abg1620